2001

Interfacial cracking in flip chip packages with viscoplastic solder deformation

Marc Heffes
Lehigh University

Heffes, Marc

INTERFACIAL CRACKING IN FLIP CHIP PACKAGES WITH...

June 2001

Interfacial Cracking in Flip Chip Packages with Viscoplastic Solder Deformation

by

Marc Heffes

A Thesis
Presented to the Graduate and Research Committee
of Lehigh University
in Candidacy for the Degree of
Master of Science

in
The Department of Mechanical Engineering and Mechanics

Lehigh University

May 4, 2001

This thesis is accepted and approved in partial fulfillment of the requirements for the Master of Science:

May 2, 2001
Date

Thesis Advisor

Chairperson of Department

Acknowledgements

I would like to thank my Advisor, Dr. Herman Nied, for his constant support. He was always there to answers all questions and to point me in the right direction. I would like to thank Dr. Ali Ayhan for his support. His research forms the basis for all the work in this thesis. The continued support of the Semiconductor Research Corp., SRC, has also been appreciated. I would also like to thank Murat Ozturk, Dennis Wang, Xiaoxian Hu, Brian Vaccaro, and Jay Goodelle for their technical support. Finally, I would like give special thanks to Ruth Dubinsky for her constant support and her help in proofreading the document.

Table of Contents

List of Figures

List of Tables

Abstract

This research examines the effect of using viscoplastic material properties in the modeling of underfill encapsulated flip chip semiconductor packages. A 3D finite element code, FRAC3D, designed specifically for the study of interfacial fracture problems was utilized and enhanced to study how viscoplastic solder material properties would effect the fracture parameters such as strain energy release rate and phase angle. Simplified two-layer models were studied to determine how they compare with fully 3D models. The results show that the two-layer slice model compared very closely with a fully 3D, model giving strain results that were only 1% different. Comparison of flip chip results with different solder material models showed that viscoplastic simulation yielded lower stress and fracture parameters when compared to plastic simulation. Overall, the viscoplastic and plastic results were similar in comparison with the linear model results.

1. Chapter 1: Introduction

1.1. Background Information

Solder joint reliability has become a key issue in the reliability of Flip Chip (FC) and Ball Grid Array (BGA) types of Integrated Circuit (IC) Packages. The use of this technology is growing tremendously. "An aggressive growth rate of 28.5 percent per year is expected to bring the flip chip market to about 2.5 billion die in 2002."[1]. This technology is used in many applications, mostly where high pin count and high speed is needed. The industry continually needs to improve package design because as chip design and computation speed improves the package becomes a bottleneck to chip performance. It was found that with one type of IC, a "50 percent improvement in logic performance for a computer system results in less than 23 percent overall gain if the package does not change"[2]

1.1.1. Introduction to different types of semiconductor packages

Trends over the last twenty years have caused many different semiconductor packages to be developed. The forces behind these developments include the demand for more leads from a single package, to decrease cost, to improve heat dissipation, smaller package size, etc. By meeting these needs many new reliability challenges have arisen.

The first package type that will be discuss is the Dual in Line Package (DIP). In a DIP the silicon die or integrated circuit (IC) is mounted on a substrate which has solid copper leads on two sides. The IC and leads are wire bonded together to make the

electrical connection. Wire bonding is the process of stringing very thin gold wires between an IC and the leads. The leads are then attached to a printed circuit board. Figure F5 shows a picture of a DIP.

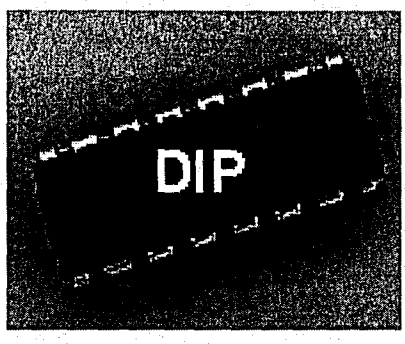

Figure 1.1 Picture of a Dual in Line Package (Courtesy of Agere Systems)

The need to increase the number of leads to a single IC has lead to the development of Quad Flat Package (QFP), which has leads on all four sides and often at a much finer pitch. A Ball Grid Array (BGA) is the third main type of IC package. This type is characterized by a grid of small (diameter $\approx$ .028 in) solder balls, which have been attached to a small copper pad on the bottom of the substrate. The BGA is then placed onto the printed circuit board (PCB), which has a set of corresponding copper pads. These parts are then heated above the solder's melting point in a reflow oven, which causes the solder to bond with the PCB.

Having a grid of solder balls allows for a much higher pin count. The number of leads on a QFP is limited by the pitch and size of a package to approximately 4L/p. The Pitch (p) is the center to center distance between two leads. L is the length of one side of the package. For a BGA, since the leads can cover the entire bottom of the package, number of leads is limited by $(L/p)^2$. This allows a BGA to have many more leads than a

QFP.

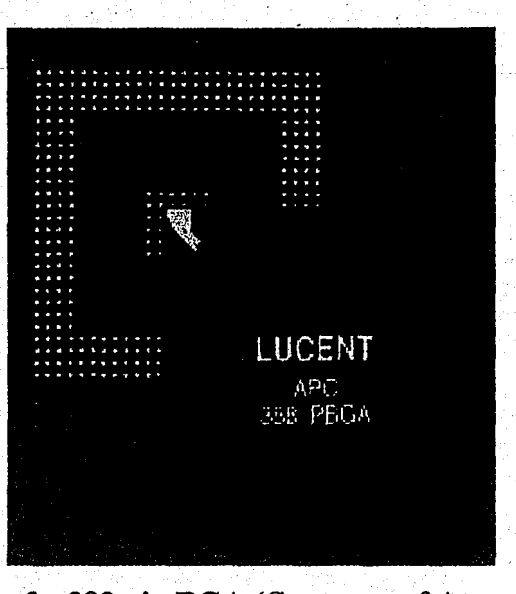

Figure 1.2 Picture of a 388 pin BGA (Courtesy of Agere Systems)

Flips chips are a subset of BGA package type. A flip chip is an IC, which has no wire bonds connecting it to the substrate. A flip chip's electrical connections to the substrate is made though an array of tiny solder bumps, on the bottom of the die, that are connected to the substrate. This whole area under the die is usually filled in with an epoxy called underfill to add strength. When this is done the package is called an encapsulated flip chip. A diagram of this is shown in Figure 1.3

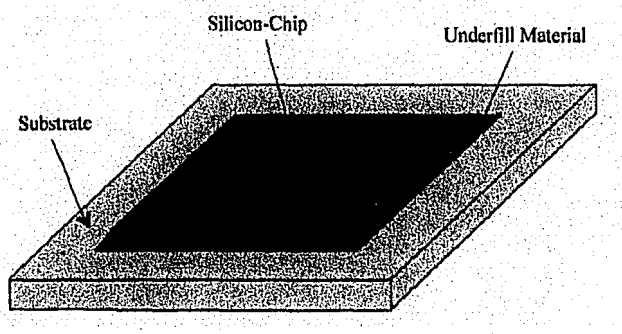

Figure 1.3 Encapsulated Flip Chip [3]

QFP.

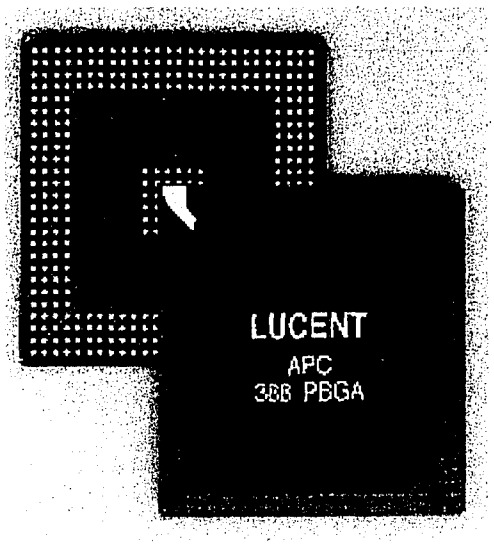

Figure 1.2 Picture of a 388 pin BGA (Courtesy of Agere Systems)

Flips chips are a subset of BGA package type. A flip chip is an IC, which has no wire bonds connecting it to the substrate. A flip chip's electrical connections to the substrate is made though an array of tiny solder bumps, on the bottom of the die, that are connected to the substrate. This whole area under the die is usually filled in with an epoxy called underfill to add strength. When this is done the package is called an encapsulated flip chip. A diagram of this is shown in Figure 1.3

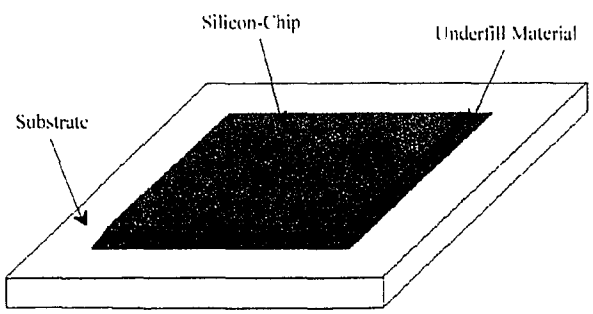

Figure 1.3 Encapsulated Flip Chip [3]

1.2. Failure modes of BGAs and Flip Chips

As BGA and flip chip technology becomes more advanced, solder joints are becoming smaller (pitch size is decreasing) and silicon die size is increasing. Also with new types of solder threatening to radically change the reliability of solder joints, it has become critical to find a way to accurately model BGAs and Flip Chips by either analytical or numerical methods. Since a BGA is very small, it is very difficult to measure strain directly, such as with a strain gauge. A method known as Moiré inferiomertry can be used, but it requires that the package be cut open in order to use this method[4]. Many feel that this invasive method changes the stress levels in the package so much that it invalidates the results. For this reason better ways of modeling BGAs and FCs has become very important to the semiconductor industry.

One main source of failure in a BGA package is at the solder joints. Solder joint failure mode is almost always by a crack initiating at the surface of the ball and propagating through the solder ball. Cracks usually occur at or near the top of the solder ball. Silicon has a low CTE (Coefficient of Thermal Expansion) relative to the other components in a package. The substrate and PCB have much higher CTE than Silicon which causes high strain/stress condition and failures at the corner solder ball under the Silicon Die edge. Once a single solder ball has failed, the package is no longer useful and therefore considered completely failed.

The solder types used for all of the studies discussed were low melting point alloys such as 62Sn36Pb2Ag, 60Sn40Pb, and 63Sn37Pb (Eutectic solder). Studies using the new lead-free solders were not examined. Eutectic solder has a melting point of

183°C. This means at room temperature, 25° C, it is at 65% of its melting point. Therefore, it is not surprising that creep is the main deformation mechanisms. Given this, it has been found that the creep rate of solder is very high. Creep in solder can cause a significant stress relaxation during high temperature dwells, even when the dwell period lasts only a few minutes.

In a flip chip, the Silicon die is attached to the substrate by underfill and tiny solder joints. The large CTE mismatch between the die and the substrate causes high stresses to often occur at the corner fillet. This can cause the interfaces to separate under high stress. This is called interfacial cracking or delamination as shown in the figure 1.4.

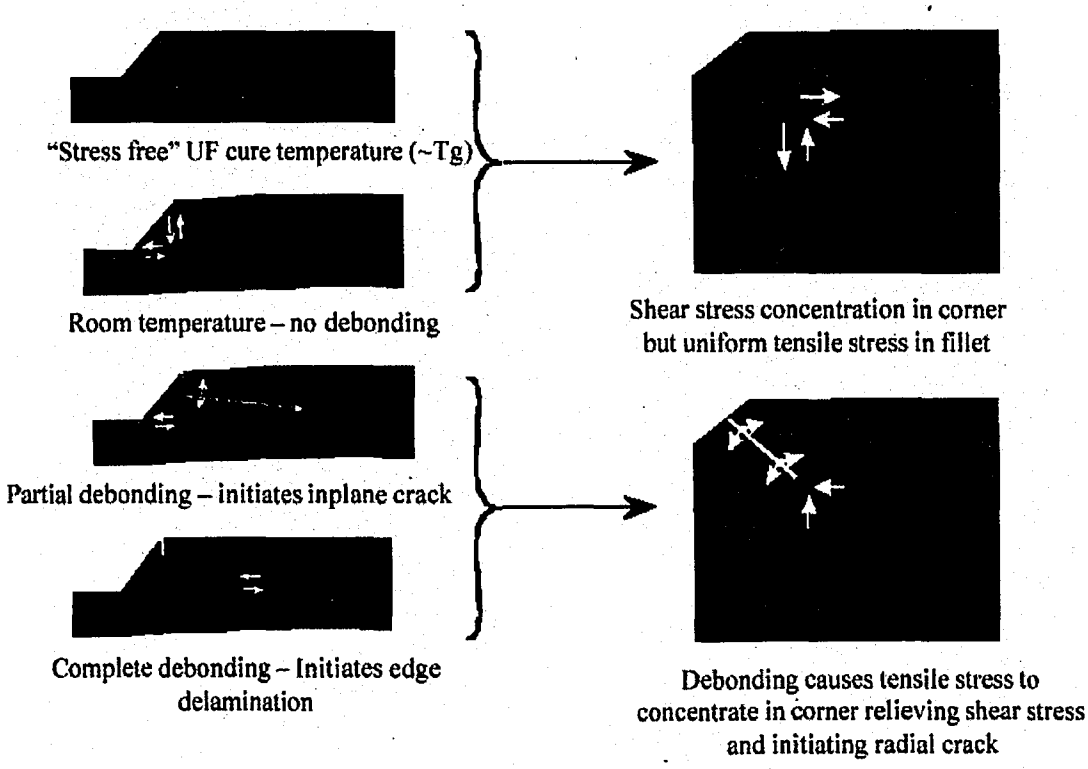

Figure 1.4 Evolution of an Interfacial Crack on the Chip/Fillet Interface (Courtesy of David Peterson, Sandia National Laboratories).

183°C. This means at room temperature, 25° C, it is at 65% of its melting point. Therefore, it is not surprising that creep is the main deformation mechanisms. Given this, it has been found that the creep rate of solder is very high. Creep in solder can cause a significant stress relaxation during high temperature dwells, even when the dwell period lasts only a few minutes.

In a flip chip, the Silicon die is attached to the substrate by underfill and tiny solder joints. The large CTE mismatch between the die and the substrate causes high stresses to often occur at the corner fillet. This can cause the interfaces to separate under high stress. This is called interfacial cracking or delamination as shown in the figure 1.4.

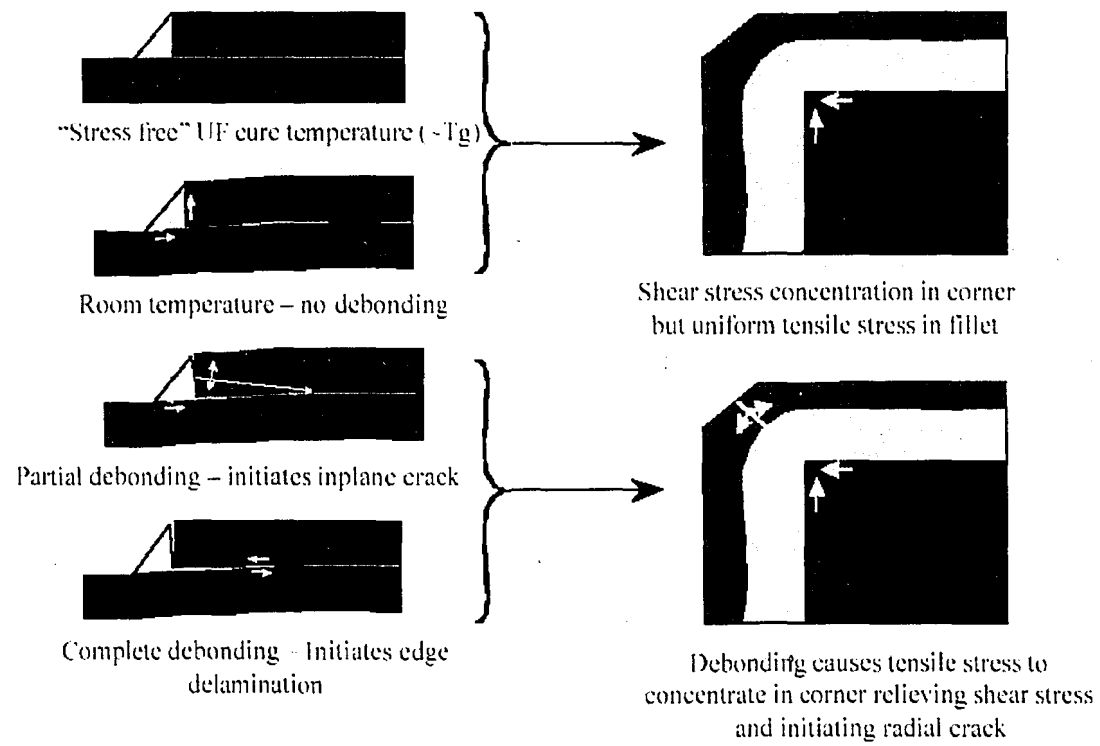

Figure 1.4 Evolution of an Interfacial Crack on the Chip/Fillet Interface (Courtesy of David Peterson, Sandia National Laboratories).

1.3. Literature overview

The topic of the reliability of solder joints in BGAs has been extensively studied for the past ten years. The work of researchers has lead to many techniques for relating analytical and numerical results to experimental data about the reliability of BGAs.

A BGA or flip chip is a very complicated device made of many layers and all "real" objects are 3D. Taking a simple straight forward approach of modeling all the known geometry of the components would lead to creation of models too complicated to create or solve within the desired time, even with today's high speed computers. The problem's complexity is compounded by the non-linearity of the properties of solder, and by cracks within the solder and between interfaces. These difficulties have lead researchers to find ways of simplifying the model of solder joints so that a solution with acceptable accuracy can be reached with a reasonable amount of time and effort.

1.3.1. Crack Models using Enriched Finite Elements

Interfacial cracks between interfaces in a flip chip have been the subject of detailed research at Lehigh. Dr. Ayhan's dissertation, [3], focused on how 3D finite elements could be enhanced to deal with cracks that occurred at the interface of two materials (interfacial cracking). This was specifically applied to a flip chip. In order to model this type of problem a unique type of finite element had to be specifically formulated to handle the stress singularity that occurs at a crack tip. This is called enriched finite elements. This type of formulation is not available in any commercial finite element software such as ANSYS or ABAQUS. For this reason a new

computational tool was developed called "FRAC3D". FRAC3D is a Finite Element program that allows for the use of Enriched 3D Finite Elements.

Many assumptions and simplifications of this very complicated system were made in order to make it manageable. Ayhan's model involves a common technique used to simplify the geometry of the system called a slice model. In a slice model only one row of solder balls is modeled. The assumption being that there are enough rows of solder balls in the system that is similar to an infinite number of rows. Non-linear analysis was incorporated for the solder, but no form of time dependency, i.e. viscoplasticity, was used. Therefore, there was no use of any time dependent plasticity or creep in the thermal cycling.

The results of this study showed that the results differed greatly from a 2D model. Although a simple slice model was used which is only partially 3D in nature. It was found for multimaterial composite structures, that the in-plane x, y directions stress components were strongly affected by how the out-of-plane, z direction, was constrained. [3]. When a crack was not added to the model it was also found that that the outermost solder ball from the center of the device had the highest stress levels and therefore was most prone to failure [3]. This research investigated how different crack lengths, shapes, and locations affected the stress and strain in solder bumps and how it affected the stress intensity factors.

1.3.2. Crack Growth Model

Since the method just described involves the use of special elements with the assumption of crack type and size, many research studying BGA and FCs have search for other methods to understand this type of problem without the complexity and additional assumptions needed for crack modeling. Many of these researches studying BGAs and FCs also used finite element analysis to model BGAs, but instead of assuming a certain flaw size and type, the model was created without any assumed flaws or cracks. Instead, the FE results of many package types were compared to experimental results done on the same packages. The packages had varied dimensions and material types, etc. The goal of these endeavors is to find a way to correlate FEA results such as stress, strain or strain energy with the experimental results, which yield only data about failure rates. Since failure rate prediction and understanding is the main goal of most research on this topic, a direct correlation is greatly desired.

1.3.3. Model specifics equations

Darveaux et al, in [5] & [6], have come up with a model that demonstrates a correlation between strain energy density and characteristic life. Their method correlates average strain energy in a single solder ball with characteristic life. Since the stress level at the edges is singular, the results are dependent on the mesh density. In order to eliminate this numerical limitation the strain energy is averaged over all the elements in a cross-section of the entire volume. By normalizing this data by the cross-sectional area of the solder ball and then regressing the FEA strain energy results with the experimental

failure results a correlation has been obtained. The resulting correlation is equation 1.1.

$$\frac{\alpha_{JOINT}}{A} = \frac{6.149 \times 10^{7} \times C}{\Delta W^{0.998}} \qquad (1.1)$$

In equation 1.1 α is the characteristic life or number of cycles till 63.2% failures in the joint population. A is the minimal cross-sectional area (in^2) ΔW is the inelastic strain energy (plastic work) per unit volume in psi or lb-in/in^3. C is the correlation error ($0.434 < C < 2.7$). [7],[8]. Darveaux et al created a correlation similar to this one, which also widely used [5],[8]. The graph in figure 1.5 shows some of the results calculated and used to obtain this correlation. As one can see, there is a definite trend, but the correlation in not as close as one might hope.

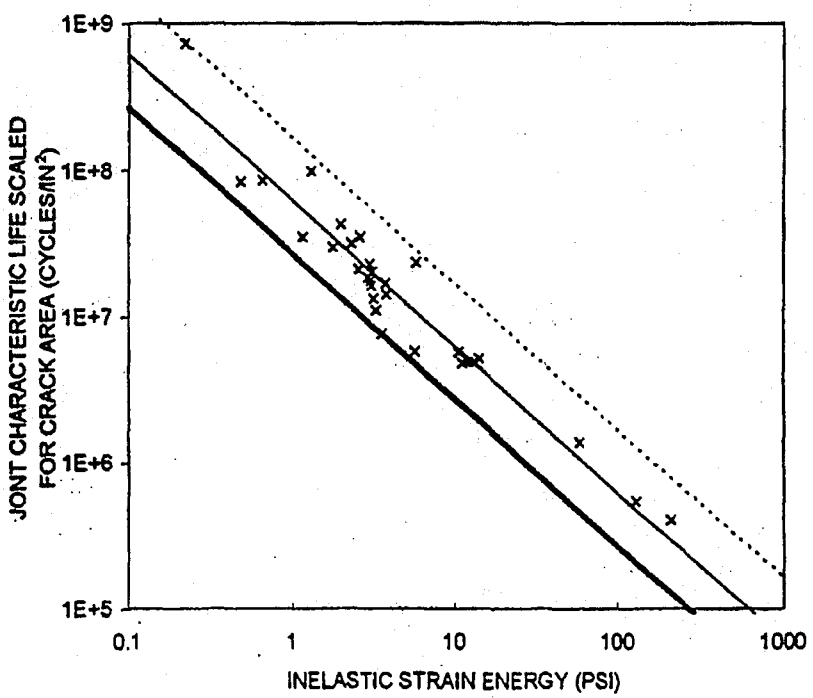

Figure 1.5 Life vs. Strain Energy [6]

1.3.4. Thermal Cycling

The type of thermal cycling used in the modeling and experiments is key to the result that will be obtain both experimentally and numerically in this type of problem. The industry standard for cycling is given in this list:

1. Ramp up to High Temperature
2. Dwell a High Temperature
3. Ramp down to Low Temperature
4. Dwell a Low Temperature

This type of thermal cycling is based on the expected thermal operating environment for electronic devices: The device in turned on causing it to heat up to a normal operating temperature. It is run for period of time (hot dwell), then shut off at which point it cools down to ambient temperature. In industry standard cycling this is approximated by linear temperature decrease. The fourth stage is to approximate a time when the device is off for a period of time (cold dwell).

1.3.5. Hysteresis Loops

Hysteresis Loops are based on the standard stress strain curves, but show the effects of cyclic loading and how stress and strain vary over one cycle. When these loops become closed it is a repeating pattern, meaning each cycle begins at the same stress and strain level and follows the same path. This happens in a solder joint cyclical loading with in 3 to 4 cycles (within a acceptable tolerance) according to [5], [9]. In most models thermal cycling is only run until the point where the loop becomes constant

because after this all data calculated would be repetitive. hysteresis loops are also one of the most important results obtained from the large amount of data and graphs that can be obtain from a model. The reason why hysteresis loops are important is because the area inside the hysteresis loop is the inelastic strain energy, ΔW, needed for the crack growth model.

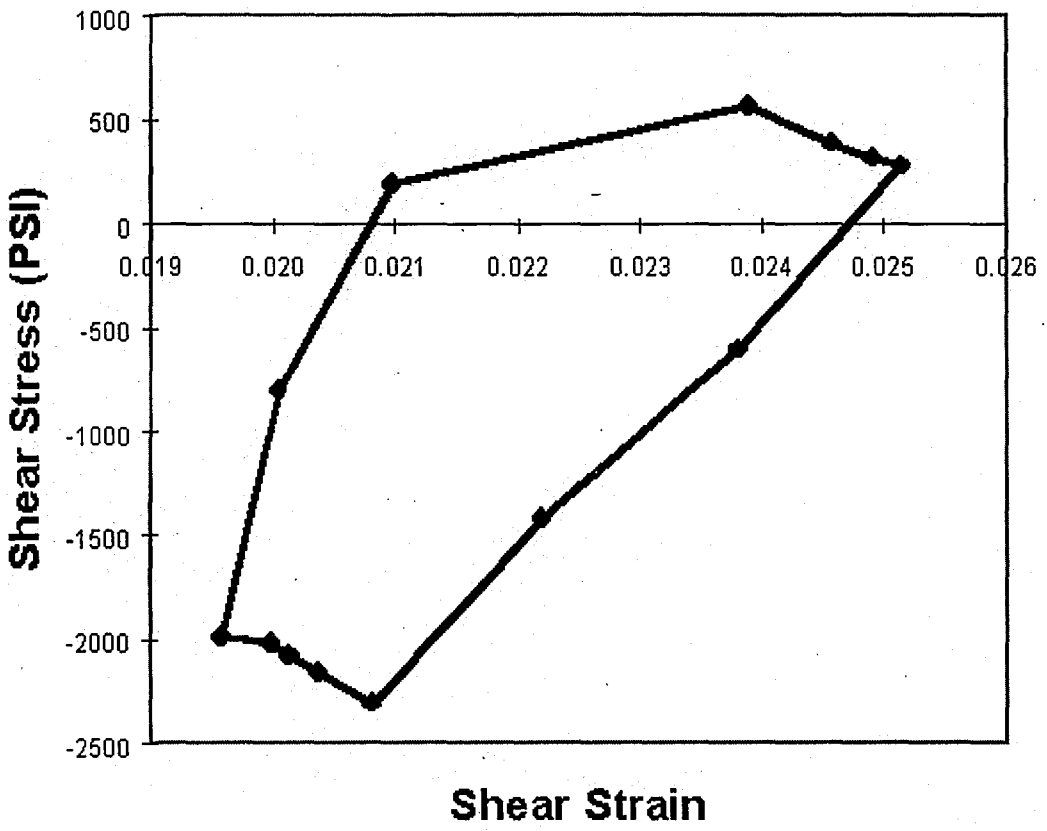

Figure 1.6 Hysteresis Loop

1.3.6. Research Implementing the crack growth model

Many papers have been written citing the use of the strain energy crack growth model pioneered by Darveaux. This section shows how different authors have implemented this method in the past. The Clech model for example does not use finite elements at all, but instead uses an analytical model. The other researchers all used FEA.

1.3.7. Solder Reliability Solutions Model

Jean-Paul Clech has published many papers describing a model he created. This model uses the material properties and geometry of the components in the system and a set of simple equations to find the effect that the Global CTE mismatch and local CTE mismatch have on stress in solder balls. Global CTE mismatch refers to the effect that differences between the CTE of PCB below the solder balls and the substrate, silicon die, and mold compound above the solder have on stressing the solder ball. Local mismatch refers to the effect caused by the CTE differences between the copper pads and the solder balls. Each solder ball is connected directly to the copper pads at both ends. In this model the temperature cycling is divided into four steps in which model properties change. The first step of the hysteresis loop system starts from a stress free, then the temperature is increased causing the stress to increase. This first step is approximated as a time independent plastic response. The second stage the hot dwell is modeled as a linear creep stress relaxation. The 3rd stage is the cold ramp. The cold ramp is modeled as time independent plastic deformation. Then 4th stage is model as time dependent creep during the dwells.[7],[8],[10]

1.3.8. ANSYS Modeling

ANSYS^{TM} commercial finite element software has been used heavily by many researchers to create 2D and 3D non linear models. Most researchers used ANSYS to create their models and mesh (preprocessing), to solve the model for the DOFs (Solution) and to analyze the displacement matrix that results for relevant data such as strain energy

(postprocessing). ANSYS allows for the use of non-linear strain analysis by viscoplasticity or elasto-plasticity, but does not have the capability to model interfacial cracking this is essential to the type of model flip chip that this research is intended to improve.

1.3.9. Finite Element Model of Solder Reliability in Literature

Beyond the work of Clech and Darveaux, many others have used similar approaches for second level reliability simulations. These have been done by many analysist, most of whom work for companies hoping to better understand and predict the reliability of their products[11],[12].

Chandran et al,[14] used the Darveaux crack growth method to test BGAs with 3 different die sizes on a 42.5 mm OLGA using FR-4 Substrate and one 400 mil die on a 32 mm OLGA. To create this non-linear finite element model, ANSYS™ was used. Slice and $1/8^{th}$ symmetry models were created using a mixture of viscoplastic and linear-elastic elements. One of the valuable conclusions was that using a global linear model, with a nonlinear submodel, greatly underestimated strain energy and plastic work. Linear elements (8-noded 3D bricks) were employed in these models [13]. Linear elements were commonly used because quadratic 20-noded viscoplastic elements are still under development by ANSYS and are not currently available. In reference [9], modeling BGAs using similar methods was employed. Anderson, et al, also found an error in ANSYS's method for calculating inelastic strain energy, which has been now corrected in the current 5.6 release of ANSYS™.

Researchers such as Pang et al [14] have used FEA and solder joint fatigue prediction models of Darveaux for underfill encapsulated flip chips. In this study a 2D plane strain model was employed. Also Clech has reported in [15] that he has adapted his model for BGA, described in section 1.3.7, to flip chips. It includes a discussion on how a flip chips "solder bumps" which are approximately 4 mils, in height, compared with BGA "solder balls" which are approximately 25 mils in height. He states that the small number of grains boundaries and flaws that exist in smaller balls decrease crack initiation, but the small cross sectional area of the solder bumps causes them to fail quicker. This study found that in flip chips with underfill, underfill delamination is the most common failure mode.

1.4. Goals of this Study

The goals of this study are to examine FE modeling for reliability analyses of ball grid arrays and flip chip types of semiconductor packages. Specifically, the effect on solder joints caused by thermal cycling including the stresses and strains cause by CTE mismatch between various components. The first goal will be to understand how different modeling techniques affect the results. A 2D plane strain model will be compared to a 3D slice model and to 3D 1/8 symmetry model. Also the differences caused by adding different types of non-linearities to the model will be studied. The results caused by using an elastic-plastic model vs. viscoplastic model on crack growth at flip chip underfill interfaces will be studied. In order to do this the existing finite element code created at

Lehigh University, FRAC3D, will be enhanced to allow for viscoplasticity. A few different package geometries will be considered including Plastic Ball Grid Arrays and Flip Chips. Actual geometry, and published material properties will be use to create 2D and 3D FEMs of BGAs and flip chips. These models will be tested with standard thermal loading conditions. The creation of some of these models will be done using the commercial FE software ANSYS™. Though ANSYS will be used at first to create models, the goal is to use FRAC3D to study interfacial cracking with creep or viscoplasticity.

2. Chapter 2: ANSYS Second Level Models

2.1. Introduction

This second chapter describes research done to study ways to improve and substantiate the validity of simpler models with fewer elements and by comparing them to larger models. Specifically, the modeling techniques used by others have been reexamined to study methods to create the simplest model without losing accuracy. It is important to remember that calculated results can not be assumed to be any more accurate than the material properties, and geometric information used. The accuracy of values for the CTE and Young's modulus for composite structures in semiconductor packaging can not be assumed to be more accurate than about +/- 10 % in most cases, see section 2.2.3. Therefore to increase the model size dramatically for example, from a runtime of 1 hour to 1 day, to change the result by 1 % is a poor use of computing resources. This chapter will therefore study the effect of dimentionality, mesh densities, and model simplification on modeling results using both linear and non-linear models.

Second level models serve as a vehicle toward this end goal. These models were created to study the effect of thermal cycling on the solder balls. Second level refers to the connection between the printed circuit board and the substrate. In a BGA, this connection is made by an array of solder balls. These connections act to carry electrical signals between the package and the circuit board and furthermore act as the only physical connection between package and the circuit board. There generally is no underfill, glue, or epoxy holding the package to the board. Since solder has a relatively low yield point

and low stress level at which creep becomes significant, there is significant plastic deformation in the solder balls during each thermal cycle. The inelastic strain energy calculations and crack growth model described earlier can eventually be used to estimate the life of BGAs, but this study will focus on the modeling techniques and not on life correlations.

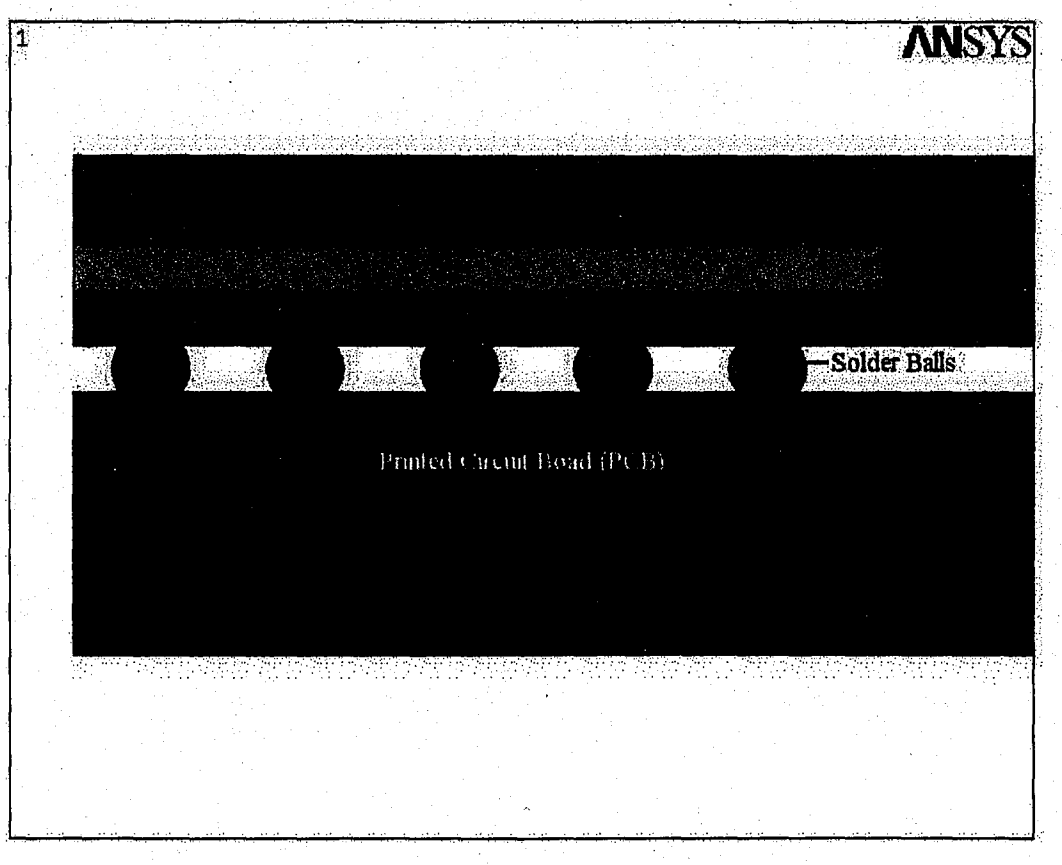

Figure 2.1 Diagram of 2D Second Level BGA Model

and low stress level at which creep becomes significant, there is significant plastic deformation in the solder balls during each thermal cycle. The inelastic strain energy calculations and crack growth model described earlier can eventually be used to estimate the life of BGAs, but this study will focus on the modeling techniques and not on life correlations.

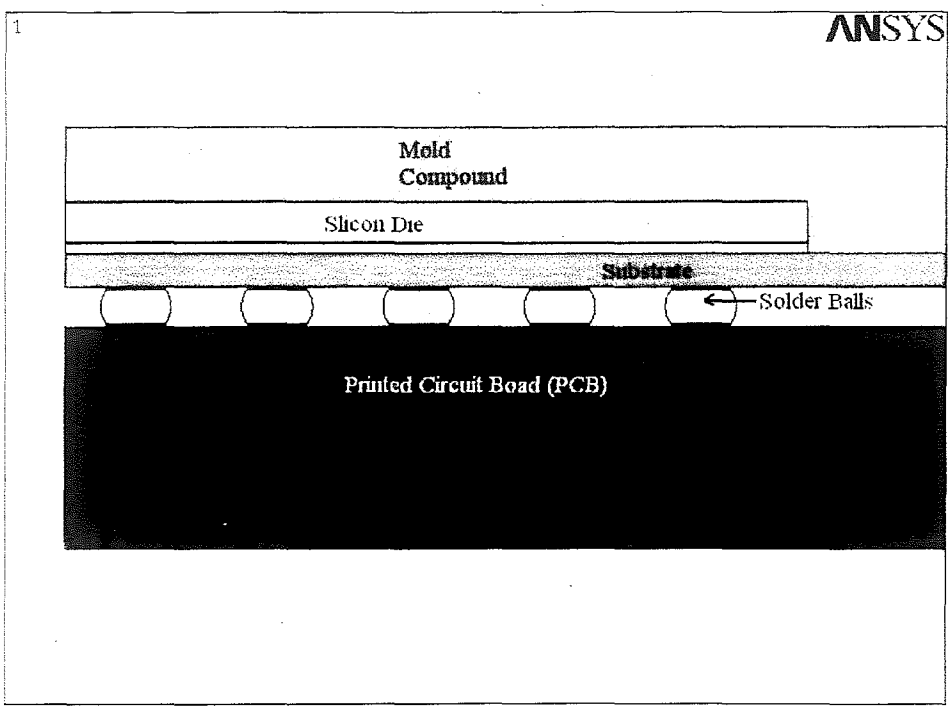

Figure 2.1 Diagram of 2D Second Level BGA Model

Table 2.1 Dimension of a 680 Pin PBGA

Feature	Size (in mils)	Feature	Size (in mils)
Die Half Diagonal	206.7	PCB thickness	90
Substrate Half Diagonal	974	Ball Pad Thickness	.10
Die Thickness	16.35	Pitch	(1 mm) 39.37
Die Attach Thickness	.85	Diagonal Pitch	55.67
Substrate Thickness	13.45	Ball Height	14
Mold Compound Maximum Thickness	51	Ball Maximum Diameter	28.08
Mold Compound Minimum thickness	30.25	Ball Pad Diameter	23.6

2.2. General Model Assumptions

The set of assumptions in this section used are common to all of models studies. These assumption make than simple enough to solve. This is needed because of the many layers in a BGA and the many connections that hold it together. As can be seen in Figure 2.1.

2.2.1. Symmetry

There is an assumed symmetry about the center of the package and along the two center lines and the two diagonals. Therefore the nodes on these lines/areas can not move off that surface. This type of symmetry also implies that the package can be divided into eight identical pieces all of which will have identical stress/strain conditions in each piece and that therefore only on 1/8 of the entire package will need to be modeled. This technique is called a 1/8 symmetry model.

2.2.2. Constraints

The bottom of PCB at the center symmetry line is completely constrained in all directions to prevent ridged body motion. In the second level models studied, the furthest node or set of nodes from the centerline were constrained at the bottom the PCB in the y direction. The assumption being that the circuit board is mounted at the corners to a rigid support. In a first level model an equivalent constraint would be to constrain the outer edge of the substrate. In pervious models studied, this was not usually done, outer edge was left free to warp. It is this researcher's believe that either assumption might be very poor, and that attaching the substrate to its second level connections, which will constrain the system only to some degree, is a more realistic condition.

2.2.3. Material properties

Material properties are of the utmost importance in a finite element model. In semiconductor models accurate material properties can be difficult to obtain. For the well understood materials in the system such as copper and silicon, obtaining these properties can be done accurately with a standard handbook. The solder material properties have been obtained only after intense study by the packaging industry. Other materials such as the substrate have the most difficult properties to obtain because they are a mixture of the composite FR-4 and copper layers, which means that they are orthotropic and need to be studied individually to obtain their properties. [16]. Also the polymer and composite materials in the structure have T_g(glass transition temperature) that are within range of temperatures studied in the model. Thus, care must be taken in the temperature dependence of the material properties of these materials. Examples of materials having a

relevant T_g are mold compound, substrate, and a printed circuit board. A list of material properties is given for reference in Table 4.2.

In this type of thermal strain problem there are two material properties that are of key importance. The first is CTE(thermal expansion coefficient) and the second is Young's Modulus. The difference between CTE of key materials such as silicon and substrate is the only force that drives the straining/stressing in the system. The Young's moduli of the key components act as the basic stiffness of the system. Basically, in the basic finite element equation [K]{D}={R}, see section 3.1 for further explanation, [K] is proportional to Young's modulus, and {R} is proportional to CTE mismatch.

In these models, all materials except solder were modeled as having linear-elastic isotropic properties. Though this may be a poor assumption for a composite like the BT substrate, accurate orthotropic material properties were unavailable.

2.3. Model Geometry and Dimensionality

This section will discuss the use of simplified geometry to approximate the system. Creating fully 3D models that capture the true geometry much better than 2D models or quasi-3D models should provide the best answer. This is because the fewest assumptions have to be made. A simple type of model that is commonly created is a 2D plane strain model. This model makes the assumption that in the out of plane direction *z* there is no strain, $\varepsilon_z = 0$ for all elements. This means that elements can not expand or contract based on the Poisson's effect or thermal expansion/contraction. This constraint

causes very high stress to be registered in the z direction. These stresses are based on a false assumption that there is no strain in the z direction. This overestimated z direction stress greatly increases the Von Mises stress. This measure or a similar measure of stress is then used as a yield criterion. Using the plane strain condition yielding is overestimated. The reason why the plane strain assumption is traditionally used is because normally one must select plane strain or plane stress as an assumption in a 2D model and it has been found that plane strain is a better assumption than plane stress for semiconductor packaging models. The other main limitation of this method is since only one cross-section can be used in a 2D model a half diagonal cross-section was use as shown in figure 2.1. By taking a different cross-section the amount of solder cross-sectional area can change dramatically which will greatly change the results. The half diagonal line used is a radial line of the solder ball, therefore the solder cross-section over estimated the amount of solder in the real system.

2.4. Constraint Equations

A non-orthodox method of relating two dissimilar materials together proved beneficial in dealing with the complex geometry found in a fully 3D Model. Normally at the interface of two materials, the mesh is allowed to remain the same on both sides. The nodes at the interface of the two materials are shared and are part of elements in both materials. This sharing can prove very difficult in a 3D model with many layers. One way is to allow a non-mapped mesh to be created allowing for a transition. The non-mapped meshes are easily created with meshing tools. This method works well in a 2D model. Even though this method creates more elements than are necessary, the model is

relatively simple having only 2 dofs u,v per node and therefore can still be easily solved. In a 3D model this is not the case. By using a meshing tool to create a tetrahedral mesh of non-rectangle shapes it was found that many more than the acceptable number of elements were created by the automatic mesher.

To deal with this problem, constraint equations were used to relate dissimilar meshing on attached surfaces. As shown in Figure 2.2. Constraint equations can be created automatically using ANSYS. This method when applied to the geometry in question seems to provide a straight forward way of dealing with varied mesh desities.

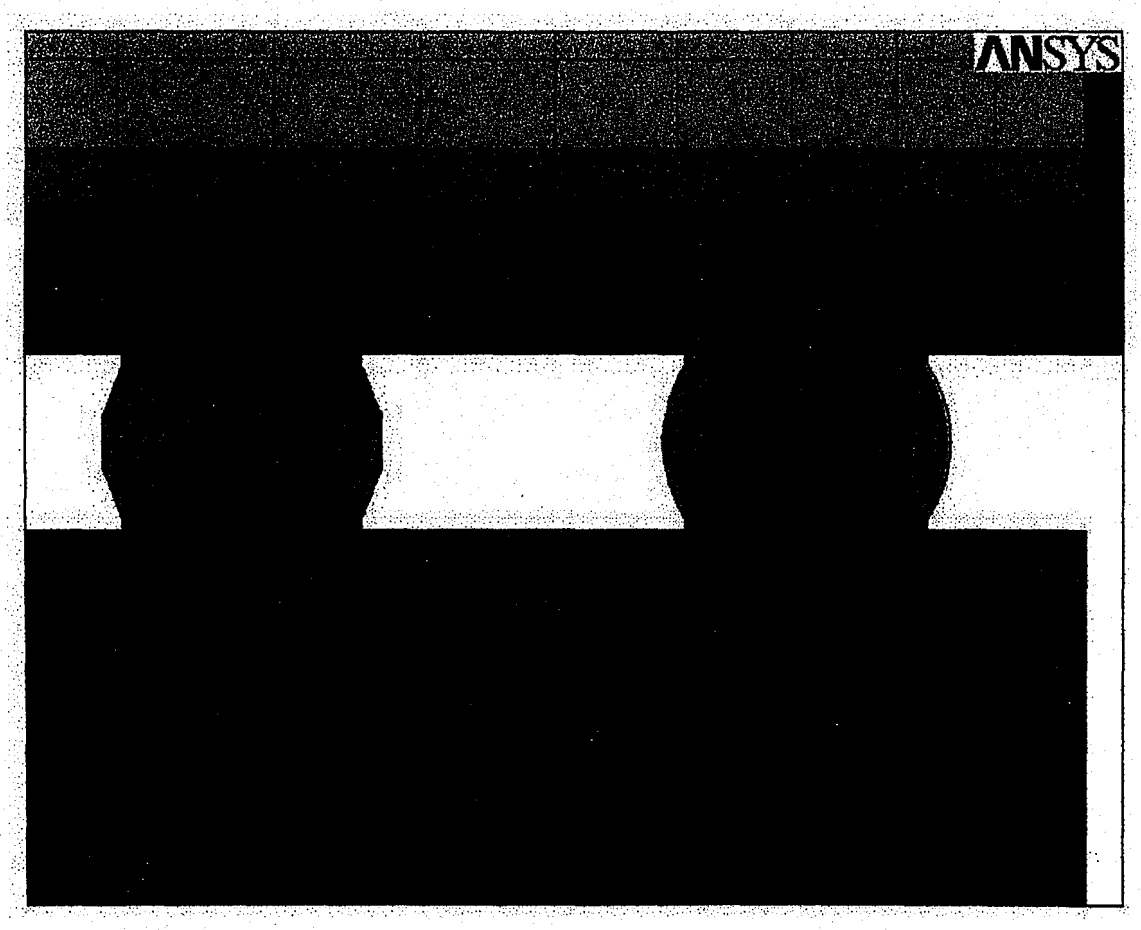

Figure 2.2 Constraint Equations Picture

relatively simple having only 2 dofs u,v per node and therefore can still be easily solved. In a 3D model this is not the case. By using a meshing tool to create a tetrahedral mesh of non-rectangle shapes it was found that many more than the acceptable number of elements were created by the automatic mesher.

To deal with this problem, constraint equations were used to relate dissimilar meshing on attached surfaces. As shown in Figure 2.2. Constraint equations can be created automatically using ANSYS. This method when applied to the geometry in question seems to provide a straight forward way of dealing with varied mesh desities.

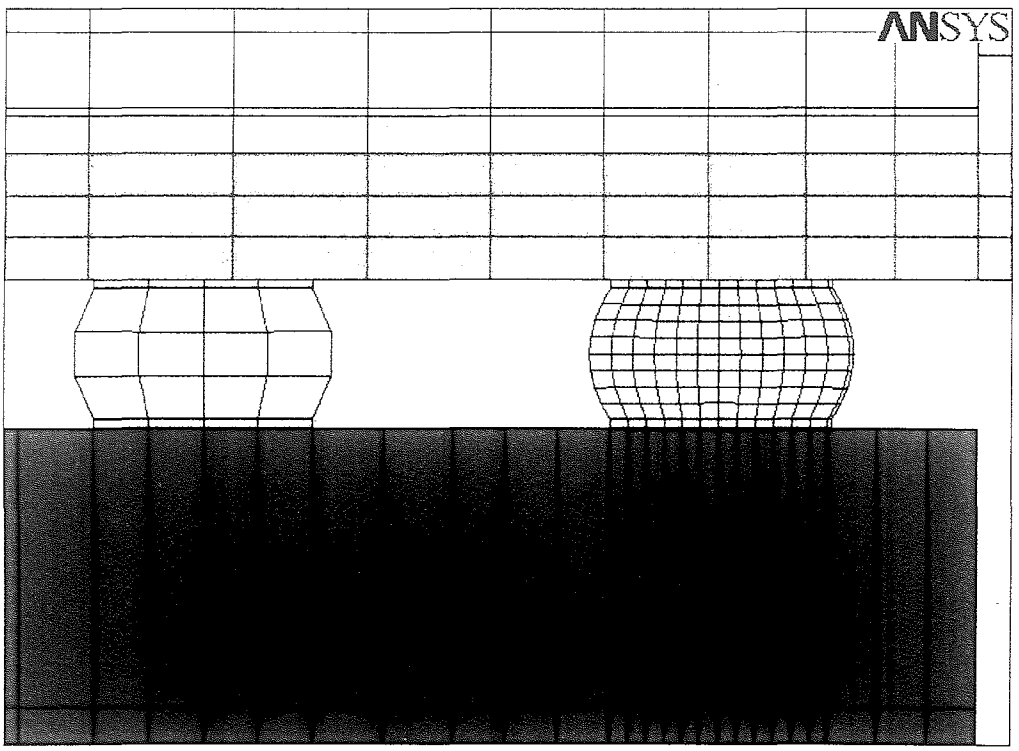

Figure 2.2 Constraint Equations Picture

2.5. Fully 3D Model

In order to test the hypothesis that simplified models are sufficiently accurate a fully 3D model was created for comparison. This model is show in figure 2.3. Given the potential level of complexity that would occur without simplification, a set of simplifying assumptions were used as follows:

1. Coarse mesh was used on all parts of the model except the critical solder ball
2. Solder balls away from the critical solder ball can be modeled as cubes with a 1 pitch by 1 pitch cross-section for which the material properties were adjusted to produce the same overall displacements
3. Constraint Equations which relate dissimilar meshes will not jeopardize the accuracy of the displacement field.
4. Simple Linear 3D brick elements will produce similar displacement fields as more accurate quadratic and cubic elements.
5. 1/8 Symmetry

All of these assumptions, except 1/8 symmetry, were tested on simpler 2D models to substantiate their validity. The added assumptions show that the changes made an insignificant difference in model results. Changing element type from quadratic to linear show the greatest change, but since ANSYS does not currently have 3D 20 noded brick viscoplastic elements available, the 8-noded brick viscoplastic elements has been used. Changes that will be described in chapter 3 will allow FRAC3D to use quadratic and cubic viscoplastic elements.

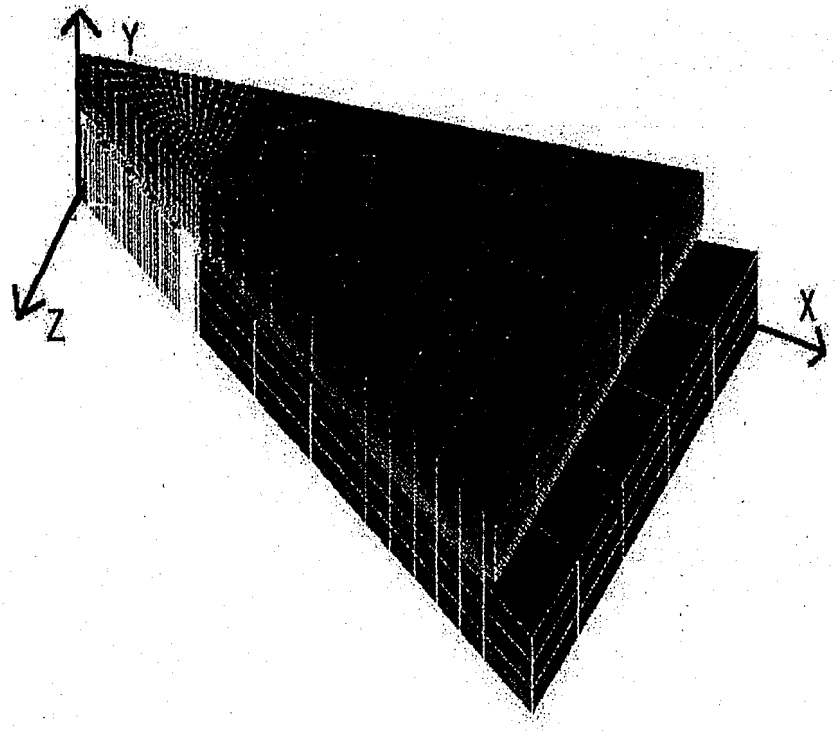

Figure 2.3 3D Model Mesh

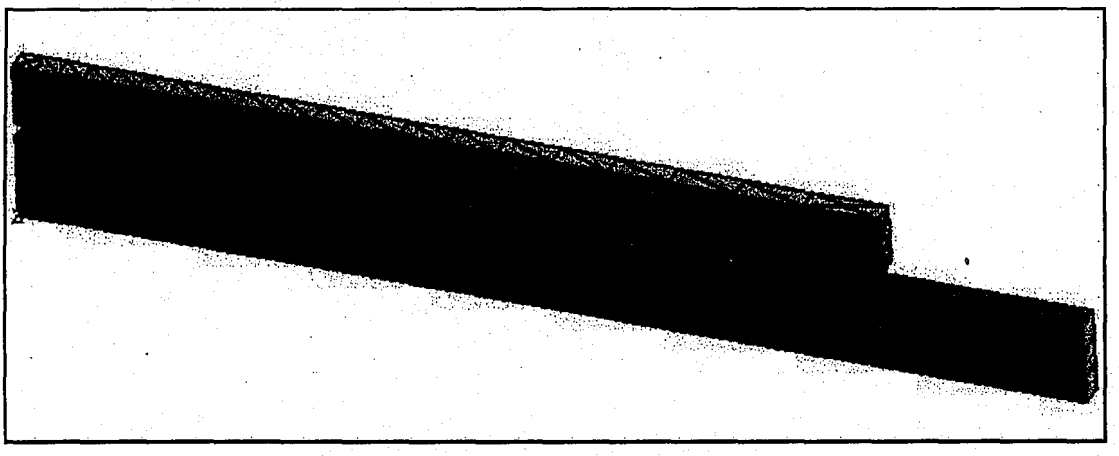

Figure 2.4 Slice Model Picture

2.6. Slice Model

The Slice model is a model where the 2D geometry is extruded one element thick. The new out of plane constraints are as follows: z direction DOF (w) is constrained such

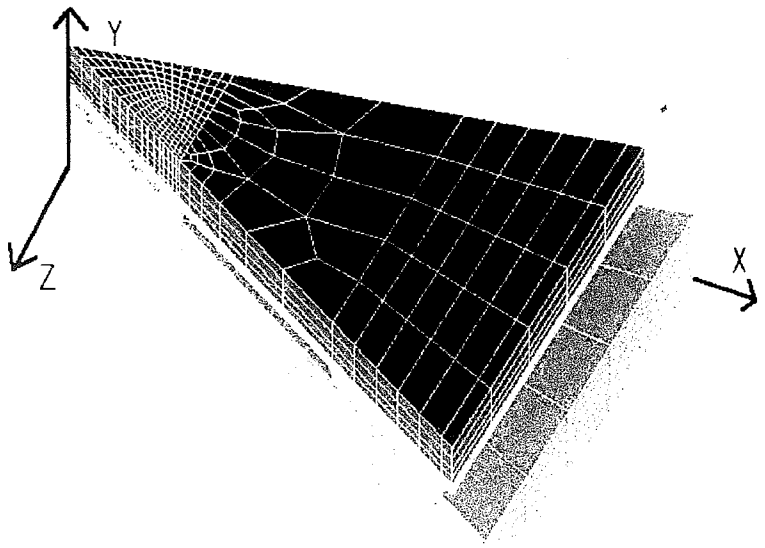

Figure 2.3 3D Model Mesh

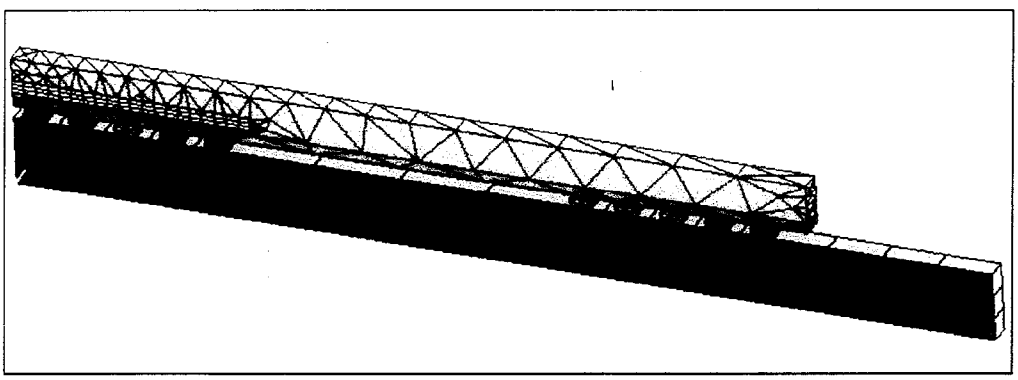

Figure 2.4 Slice Model Picture

2.6. Slice Model

The Slice model is a model where the 2D geometry is extruded one element thick. The new out of plane constraints are as follows: z direction DOF (w) is constrained such

that all nodes on back surface are fixed in the z direction (w=0) and all nodes on the front surface are coupled in the z direction. Coupled nodes means that all of the nodes in the coupled set have the same displacements in a specified direction ($w_1 = w_2 = w_3 = w_4 \ldots$) This type of out of plane constraint is called the generalized plane strain method. The goal of this method is to eliminate the over constraining effect caused by plane strain assumption. Figure 2.4 shows the mesh of a slice model.

2.7. Layered Slice Model

This model is similar to that of the slice model except that instead of having a model that is one element thick a model that is two elements thick is created. The first layer is the same as the Slice Model, but the second layer added contains no solder elements only the surrounding system is modeled: Die, substrate, PCB etc. This is done to account for the grid effect, which produces correct solder volume.

The thickness of the two layers is determined using formula 2.2 and 2.3.

Solder Extrusion: $D_1 = \frac{\pi}{2} r$ (2.1)

Second Extrusion: $D_2 = p - D_1$ (2.2)

Where r is the average radius of a solder ball and p is the pitch distance such as 1 mm.

In the literature, strip models that are similar to this have been used, but they often differ in that they try to account for the true shape of solder balls by revolving the solder balls into axisymmetric shapes instead of an extruded shape[6],[13]. This may give a more accurate answer but it much more difficult to mesh. The beauty of the slice model

and the Layer Slice model is that are much easier to create and mesh than a Strip model. In fact a simple file containing modeling and mesh routines has been created to change a 2D plane strain model in a layered slice model.

2.8. Conclusions and Results

A summary of the results is given here in Table 2.2 The results confirmed the hypothesis made based on descriptions of models in the pervious section. That the 2D plane strain model shows significantly higher stress and strains than the Fully 3D model. Also, as expected, the slice model underestimate stress and strain in the solder joints. The best result set of simplified results came from the layered slice model, which produce results that were not significantly different from that of the Fully 3D model. This is an important result because it allows for packages with this type of symmetry and connection grid to be modeled much more simply with much less model creation time and less model run time. As a rough estimate, the model creation time and run time for layered slice were both be about ¼ as long as that of a fully 3D model.

Table 2.2 Linear Analsys Results

	PBGA Models using different modeling Assumption				
	2D Model Quadratic elements	2D Model with Linear elements	Slice Model	Two Layered Slice	3D 1/8 Symmetry model
Num. of elements	1634	1653	n/a	n/a	4203
Num. of nodes	4860	1830	n/a	n/a	6074
Num. of dof	2	2	3	3	3
# dof eqns	9720	3660			18222
Strain*	0.00189	0.00201	0.00138	0.00172	0.00173
% difference from 1/8 sym. model	9.41%	16.02%	-20.15%	-0.91%	0.00%

*Average 1st principal direction Strain in solder ball under die edge

3. Chapter 3: Finite Element Method Applied to Fracture and Viscoplastic Problems

This thesis focuses on how the finite element method(FEM) can be enhanced to allow for interfacial cracks and the use of viscoplastic material properties. These concepts and the formulation for this method will be presented and the key concepts will be explained.

3.1. Basic Finite Element Formulation for 3D Linear Solid Mechanics Problems

In this section the basic formulation that is used to solve linear elastic 3D problems will be explained with no provisions for singularities or non-linear material properties. This is just an overview of the basic equations used. A more detailed discussion of the finite element method as presented here can be found in many books including [18] and is taught in many undergraduate and graduate level classes in engineering because this method has become a standard for solving engineering problems.

In a solid mechanics problem, the variables of state which define deformation, stress and strain is the displacement field of all points with in the structure studied. In the FEM the displacement field is approximated by calculating the displacement at a finite number of points within the structure known as nodes. At each node there are degrees of freedom(DOFs) each one is a scalar variable denoting the displacement in one direction. In a 3D problem, there are 3 DOFs per node denoted as u, v, and w. In order to solve for the DOFs a standard equation show in 3.1 is used [17].

$$[K]\{D\}=\{R\} \quad (3.1)$$

Where [K] is the global stiffness matrix(square and symmetric), {D} contain DOFs for all nodes in a column matrix and {R} contains the forces and loads causing the displacement. In order to calculate stiffness and forces at the nodes, the nodes are grouped into elements which can be thought of as the building blocks of a structure. For 2D problems, elements are usually quadrilaterals or triangles and for 3D problems cubes and tetrahedrons are often used. Figure 3.1 shows a 20-noded quadratic 3D elements of the type that will be use in this study.

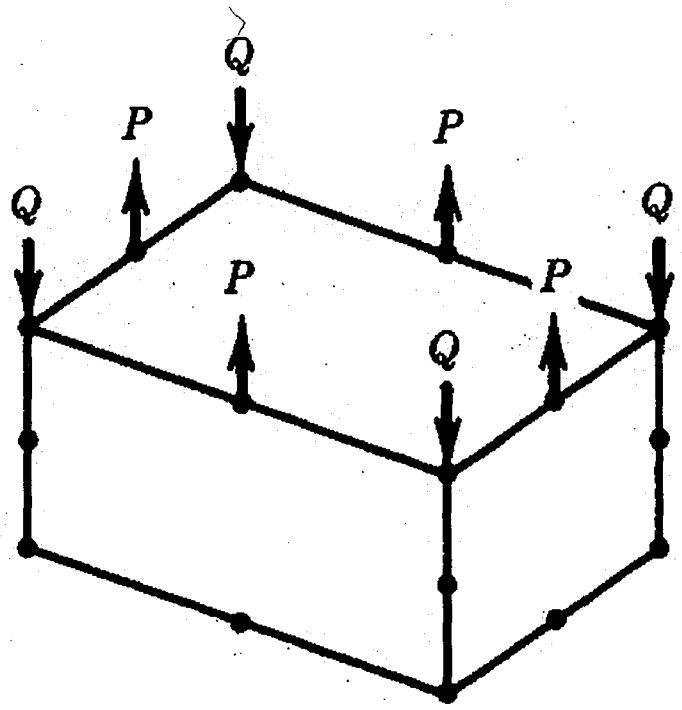

Figure 3.1 20 Noded Element with Constant Stress Load [18]

For a single element the element stiffness matrix, [k], and element force matrix {r} are calculated using a method known as the Rayleigh-Ritz method that is base on the concept that system will always be in equilibrium at displacement values that minimize the potential energy of the system. Equation 3.2 gives the standard form for potential energy in a solid mechanics problem.

$$\Pi_p = \int_V (\frac{1}{2}\{\varepsilon\}^T[E]\{\varepsilon\} - \{\varepsilon_o\}^T[E]\{\varepsilon_o\} + \{\varepsilon\}^T\{\sigma_o\})dV - \int_V \{u\}^T\{F\}dV - \int_S \{u\}^T\{\Phi\}dS - \{D\}^T\{P\} \quad (3.2)$$

Where ε is strain, σ is stress, ε_0 and σ_0 are initial strain and stress, [E] is the elastic material properties matrix, {u} is the matrix of displacements, F is the body forces matrix, Φ is surface tractions matrix, and P is concentrated load matrix. By taking the derivative of this matrix equation with respect to all the DOFs and setting this equal to zero we get the standard finite element formulation which is used calculate [k] and {r} described earlier. Once [k] and {r} are found for all elements they are assembled into the two large matrices [K] and {R},[18].

$$[k] = \int [B]^T[E][B]dV \quad (3.3)$$

$$\{r_e\} = \int_{Ve} [\mathbf{B}]^T[E]\{\varepsilon_o\}dV - \int_{Ve} [\mathbf{B}]^T\{\sigma_o\}dV + \int_{Ve} [N]^T[F]dV + \int_{Se} [N]^T[\Phi]dV \quad (3.4)$$

Equation 3.3 and 3.4 contain two matrices that are central to finite element formulation, [N] which is the shape function matrix and [B] which is the strain displacement matrix. The shape function, [N], relates the DOF values which give the displacement at points to an approximate displacement field which gives displacement of all points with in an element[18]. Figure 3.2 shows how a continuous function is created form a dof quantity such u , v or w. This figure shows the displacement field if a value of 1 is assigned at node #1 and a value of 0 is assigned for all other nodes.

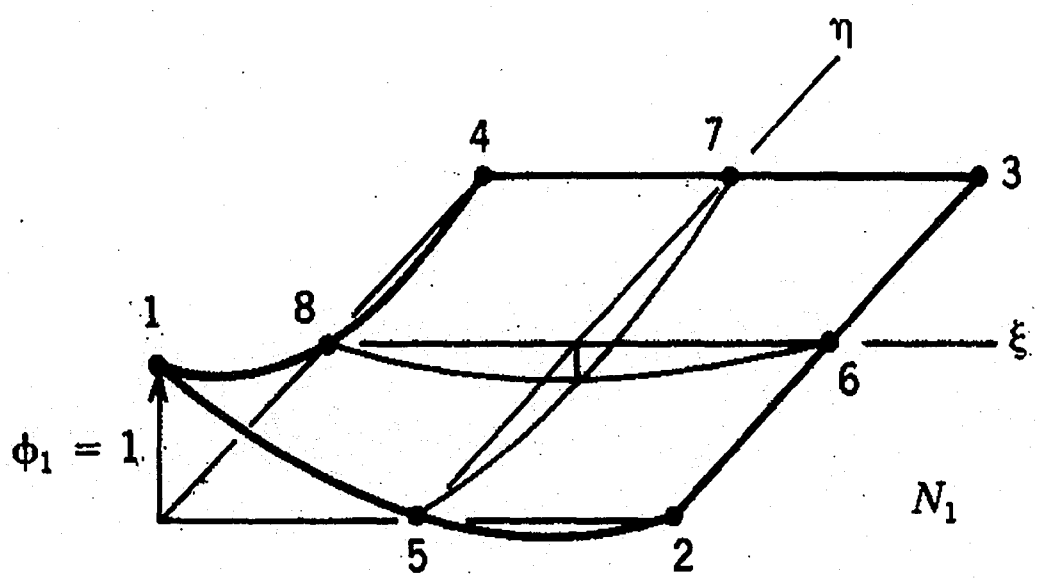

Figure 3.2 Graphical Representation of Shape Function [18]

By taking the derivative of shape functions with respect to x, y and z in the manner shown in equation 3.5, in the following matrix which relates the DOF values to the six strain quantities for 3D problems is created.

$$[\partial] = \begin{bmatrix} \partial/\partial x & 0 & 0 \\ 0 & \partial/\partial y & 0 \\ 0 & 0 & \partial/\partial z \\ \partial/\partial y & \partial/\partial x & 0 \\ 0 & \partial/\partial z & \partial/\partial y \\ \partial/\partial z & 0 & \partial/\partial x \end{bmatrix}, \quad \begin{Bmatrix} \varepsilon_x \\ \varepsilon_y \\ \varepsilon_z \\ \gamma_{xy} \\ \gamma_{yx} \\ \gamma_{zx} \end{Bmatrix} = [\partial] \begin{Bmatrix} u \\ v \\ w \end{Bmatrix}, \quad [B] = [\partial][N] \qquad (3.5)$$

So from equation 3.5, which defines [B] it is shown that the equation for strain is equation 3.6.

$$\{\varepsilon\} = [B]\{d\} \qquad (3.6)$$

From the strain formula in equation 3.6, it is a simple extension for linear elastic problems that the stress state can be obtained by equation 3.7.[18]

$$\{\sigma\}=[E][B]\{d\} \qquad (3.7)$$

3.1.1. Stress Computation and Gauss Quadrature

In order to integrate these expressions numerically a finite number of points must be picked to evaluate the function. A widely use scheme for integrating is Gauss Quadrature. In this scheme very few points are needed to integrate the expression if the proper weighting is given to the values at these points. For example if the function is integrated along the ξ axis form –1 to 1 and 3rd order quadrature is used the function is only evaluated at 3 points +/- .577 and 0 which are weighted 5/9 and 8/9 respectively. These points are called Gauss points. If a 3D element with 20 nodes is used, 3rd order Gauss Quadrature gives reasonably accurate results and 27 Gauss points will be needed for each element.

When stresses are calculated with in an element they are most accurate at the points that were actually used to create the stiffness matrix. So stress and strain calculations at Gauss points are used as an alternative to nodal point to determine a more accurate stress field. This becomes critical in how stress and strain are calculated in non-linear problems [18].

3.2. Enriched Finite Elements

In this study, improvements on the models used previously to create interfacial crack will be made. In a previous study [3], Ayhan determined the formulation for Enriched Finite Elements to study three-dimensional homogeneous and bi-material crack problems. Since this formulation will be used in this study as well, it is summarized here. Basically, in the model the nodes at the crack tip are specified. Classical fracture mechanics can then be used to deal with the singularity that occurs at the crack tip. The output of this formulation is strain energy release rate, G and the different stress intensity factors, which give the strength of each mode of crack opening. Using experimental data this G value can be used to determine likelihood and rate of crack growth. The 3 equations labeled (3.8) form the basis for determining G and stress intensity factors, K at an interfacial crack tip. The quote below describes these equations and some of the specifics of Enriched Finite Elements.

$$u(\xi,\eta,\rho)=\sum_{j=1}^{nodel}N_i(\xi,\eta,\rho)u_j+Z_0(\xi,\eta,\rho)\sum_{i=1}^{4}N_i(\eta)K_I^i\left(f_1(\xi,\eta,\rho)-\sum_{j=1}^{nodel}N_j(\xi,\eta,\rho)f_{1j}\right)$$
$$+Z_0(\xi,\eta,\rho)\sum_{i=1}^{4}N_i(\eta)K_{II}^i\left(g_1(\xi,\eta,\rho)-\sum_{j=1}^{nodel}N_j(\xi,\eta,\rho)g_{1j}\right)$$

$$v(\xi,\eta,\rho)=\sum_{j=1}^{nodel}N_i(\xi,\eta,\rho)v_j+Z_0(\xi,\eta,\rho)\sum_{i=1}^{4}N_i(\eta)K_I^i\left(f_2(\xi,\eta,\rho)-\sum_{j=1}^{nodel}N_j(\xi,\eta,\rho)f_{2j}\right)$$
$$+Z_0(\xi,\eta,\rho)\sum_{i=1}^{4}N_i(\eta)K_{II}^i\left(g_2(\xi,\eta,\rho)-\sum_{j=1}^{nodel}N_j(\xi,\eta,\rho)g_{2j}\right)$$

$$w(\xi,\eta,\rho)=\sum_{j=1}^{nodel}N_i(\xi,\eta,\rho)w_j+Z_0(\xi,\eta,\rho)\sum_{i=1}^{4}N_i(\eta)K_{III}^i\left(h_2(\xi,\eta,\rho)-\sum_{j=1}^{nodel}N_j(\xi,\eta,\rho)h_j\right)$$

Crack Displacement Field Equations **(3.8)**

"In the formulation of displacement field for the enriched crack tip elements, additional unknowns (stress intensity factors) are included as separate degrees of freedom, i.e (3 stress intensity factors for each crack tip node). The contributions from these stress intensity factors are then assembled into the global matrix as unknowns in the same way it is done for the regular elements. The first summation terms in Eq.'s (3.1)-(3.3) represent the usual displacements as formulated in regular isoparametric elements. Z_0 is a "zeroing function" that provides inter-element compatibility between the crack tip elements and the elements that surround the enriched elements.

The zeroing function corrects any inter-element displacement incompatibility that may arise due to non-polynomial singular strain field defined in the enriched crack tip elements. K^i_I, K^i_{II}, and K^i_{III} 's are the unknown stress intensity factors, for mode I, mode II, and mode III, respectively. The functions f_1, f_2, g_1, g_2, and h are the asymptotic displacement terms that are coefficients of the mode I, mode II and mode III stress intensity factors. The terms f_{1j}, f_{2j}, g_{1j}, g_{2j}, and h_j are the asymptotic displacement expressions evaluated at the jth node in the element."[3]

3.3. The Theory of Viscoplasticity

Viscoplasticity is a material model in which the permanent deformation that occurs is time dependent. Central to the idea is that there exists a time derivative of strain called strain rate, which is a function of material type, stress and temperature conditions. In fact, all materials have some level of viscoplasticity, but for most the rate is so slow that it becomes negligible. This phenomenon is often called creep and as a rule of thumb it is only a significant effect for material above ½ their melting temperature based on an

absolute temperature scale. For some materials like steel the rate might be measured in years for other materials such as solder in may be measured in minutes or seconds.

The mechanism for viscoplasticity is complicated and not fully understood, consequently like most other materials data it is arrived at by empirical results. It is known that viscoplastic strain rate is a function of stress condition, time, temperature and strain history (strain hardening/softening). Most empirical relationships isolate one or two of these parameters and study a few materials so that empirical constants can be found by curve fitting. The creep relationship in equation 3.9 and 3.10 are examples found in literature[19].

$$\dot{\varepsilon} = ae^{-Q/RT} \text{ (Mott, 1953)} \qquad \textbf{(3.9)}$$

$$\dot{\varepsilon} = ae^{b+c\sigma} \text{ (Nadai, 1931)} \qquad \textbf{(3.10)}$$

As can be seen from these relationships strain rate is usually characterized by a highly non-linear function and often an exponential function of stress and temperature. For metals, creep relationships are most often found using a one-dimensional (tension) test. Very precise equipment is used that holds the stress and temperature of the sample constant over a long period of time. These tests usually show that the constant stress creep curve divided into three stages based on time. These stages are the primary stage, steady state stage, and tertiary stage. In the primary stage there is strain hardening just as

in plasticity until a steady state is reached. Figure 3.3 shows a common graphical representation of this.

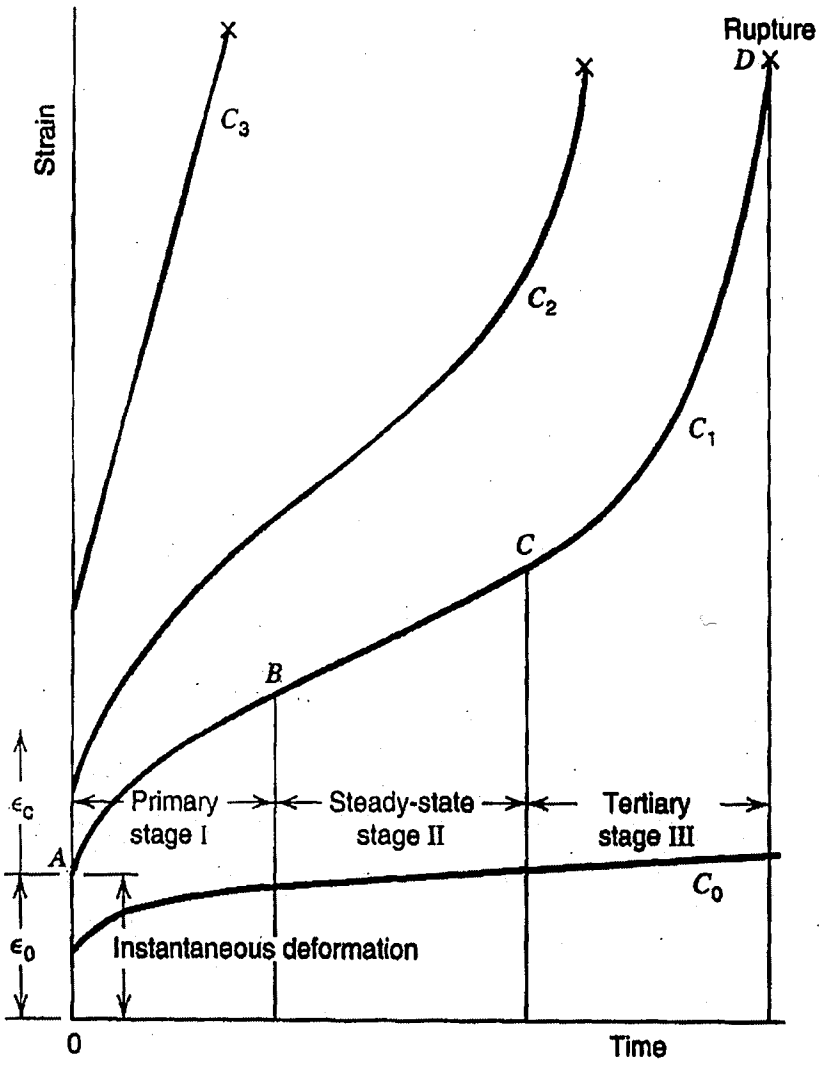

Figure 3.3 Graph showing 3 Regions of Creep Curve [19]

3.3.1. Viscoplastic Correlations for Solder

Since solder is such an important material to electronic packaging problems, much research has gone into determining a strain rate correlation that can be used to accurately fit solder's behavior and to determine the accurate empirical constants. In Lau [2],

extensive testing that includes results for five different solder alloys. All five alloys are curve fitted to the equations in 3.11, which allow for strain hardening so that both primary and steady state creep is accounted for. In equations 3.11, $\frac{d\varepsilon_c}{dt}$ is the strain rate, σ is the effective stress, ε_{VP} is viscoplastic strain, and T is the absolute temperature in Kelvin.

$$\frac{d\varepsilon_s}{dt} = C_1[\sinh(C_2\sigma)]^{C_3} \exp(-C_4/T)$$
$$\frac{d\varepsilon_c}{dt} = \frac{d\varepsilon_s}{dt}\left(1 + C_5 C_6 \exp(-C_5 \bar{\varepsilon}_{VP})\right) \qquad \textbf{(3.11)}$$

Table 3.1 Solder Flow Rule Constants

	Units	SN60Pb40	62Sn36Pb2Ag
C1	1/sec	1.61E+05	8.03E+04
C2	1/PSI	4.62E-04	4.62E-04
C2	1/Mpa	0.067007	0.067007
C3		3.3	3.3
C4	Deg K	8112	8112
C5		698	263
C6		0.015	0.023

In order to model the actual strain rate as a function of stress and temperature, creep correlations have been used by many researchers. Specifically, the steady state creep relation shown in Equation 3.12, also known as Anand's model for time dependent plasticity, has been heavily used because it can be used as a standard part of ANSYS. The constants used are based very closely on the correlation described in the previous section to experimental results done on solder balls[2]. It was used by Darveaux et al in

their models [5], [6], [13]. Anand's model will not be used in this study. The correlations taken directly from the research in [2] will be used because they are simpler and more accurately match the data.

In Anand's model, plasticity and creep are combined into one phenomenon. Equation 3.12 shows the basic formula it also involves three evolution equations that are needed to determine strain hardening by changing the s term.

$$\frac{d\varepsilon_p}{dt} = A\left[\sinh\left(\xi\frac{\sigma}{s}\right)\right]\exp\left(\frac{-Q}{kT}\right) \qquad (3.12)$$

Where $\frac{d\varepsilon_p}{dt}$ is the plastic/creep strain rate. σ is the effective stress and T is the absolute temperature in Kelvin. ξ and m are dimensionless constants. Q is the activation energy, k is the Maxwell Boltzman constant and s is a stress constant.

3.4. The Formulation of Viscoplasticity in FEA

The formulation used in this study for the implementation of Viscoplasticity is based on Owen and Hinton's book[20]. In this model, strain is divided into 3 parts elastic, thermal, and viscoplastic.

$$\varepsilon_T = \varepsilon_e + \varepsilon_{Th} + \varepsilon_{VP} \qquad (3.13)$$

In finite elements the derivative of the displacements gives the total strain as:

$$\varepsilon_T = [B]d \qquad (3.14)$$

When only elastic strains are considered this serves as the only equation needed to determine the complete strain picture. The force vector {R} contains only real forces,

which are specified explicitly in the model input such as concentrated nodal loads and surface pressure.

When thermal strains are added the total strain changes without a change in the stiffness or exterior forces of the structure. Since finite element method always involves a set of equation written in the matrix form, [K]{D}={R}, the formulation needs to be changed within this context. Thermal strains are represented by adding forces to the {R} term as follows. In equations 3.15 and 3.16, α is CTE , T is temperature, F represents a force vector, and V is volume.

$$F_t = \int_V B^T E \varepsilon_{Th} dV, \qquad where \qquad \varepsilon_{Th} = \alpha \Delta T \tag{3.15}$$

The formulation for the viscoplastic strain is more complicated and is explained in the next section, but once it is obtained it is straightforward to add it to the finite element formulation. It is added in the same way as thermal strain. The formulation can be summarized by the following set of equations (3.16).

$$\{R\} = F_{Applied} + F_{Th} + F_{VP} \qquad \begin{array}{ll} F_{Applied} = \sum r_e & \text{Equation 3.4} \\ F_t = \int_V B^T E \varepsilon_{Th} dV & \varepsilon_{Th} = \alpha \Delta T \\ F_{VP} = \int_V B^T E \varepsilon_{VP} dV & \varepsilon_{VP} \text{ from interative process} \end{array} \tag{3.16}$$

F_{VP} is a pseudo force that does not exist in the real material. Therefore, when calculating the stress, both the effects of thermal strain and viscoplastic strain must be subtracted. So the formula for stress becomes equation 3.17.

$$\boldsymbol{\sigma} = \mathbf{E}(\mathbf{Bd} - \varepsilon_{Th} - \varepsilon_{vp}) \tag{3.17}$$

The forces in the F_{VP} vector are used to change the total strain which is the actual effect caused by the viscoplastic material behavior.

3.4.1. Determining Strain Rate at a Point

All calculations of strain rate are calculated at the gauss points to allow for higher accuracy and simpler integration of the pseudo loads. The strain and stress vector for any point in a 3D problem has six components: *xx, yy, zz, xy, yz, xz*. But a strain rate empirical correlation is almost always given from a uni-axial test, in which stress and strain become scalar quantities. In order to reconcile this difference, we must define two new variables to use in the system. The first is F, which is the equivalent stress. In this study F is always the Von Mises stress arrived at by equation 3.18

$$F = \sqrt{\tfrac{1}{2}[(\sigma_1 - \sigma_2)^2 + (\sigma_2 - \sigma_3)^2 + (\sigma_3 - \sigma_1)^2}} \qquad \textbf{(3.18)}$$

The second variable, **a**, that will be needed is a special unit vector which gives the relative magnitudes of non-linear strain in each direction. It is based on the assumption that the overall volume can not change from plastic straining.

$$\vec{\mathbf{a}}^{\mathrm{T}} = \frac{\partial F}{\partial \sigma} = \left[\frac{\partial F}{\partial \sigma_x} \quad \frac{\partial F}{\partial \sigma_y} \quad \frac{\partial F}{\partial \sigma_z} \quad \frac{\partial F}{\partial \sigma_{xy}} \quad \frac{\partial F}{\partial \sigma_{xz}} \quad \frac{\partial F}{\partial \sigma_{yz}} \right] \qquad \textbf{(3.19)}$$

Now with these two variables defined, one can change any scalar strain rate function into a new vector function. If the strain rate function is of the form in Equation 3.20, where σ and T are scalars, it is subsequently changed into the vector form in Equation 3.21. In

this way the six directional vector $d\varepsilon_{vp}/dt$ can be obtained using correlations that are taken from experimental results.

$$d\varepsilon/dt = f(\sigma,T) \qquad (3.20)$$

$$d\varepsilon/dt = f(F,T)\mathbf{a} \qquad (3.21)$$

3.4.2. Determination of Viscoplastic Strain

Since the viscoplastic strain is non-linear and time dependent, the solution must be arrived at by an iterative process. With two important loops, the first being one in which the loads are incremented as in standard incremental plasticity. In the second loop time stepping occurs. At each time step the strain rate is evaluated based on a specific empirical formula and then the viscoplastic strain in incremented. The flow chart in Figure 3.5 helps to clarify this iterative process.

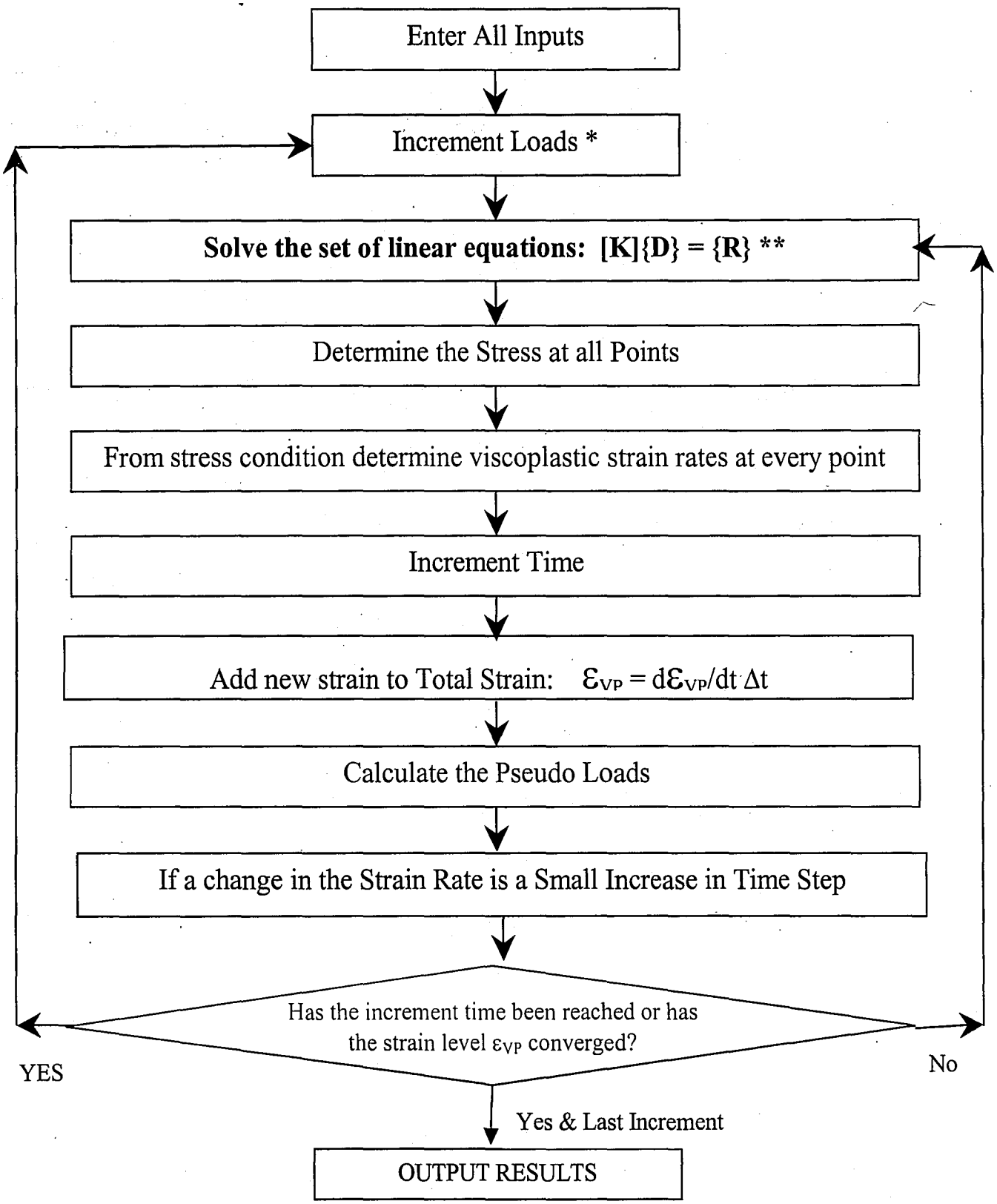

Figure 3.4 Flow Chart of Viscoplastic Calculations

---

* Incrementing is done using by simply dividing total load into evenly sized steps.

** Solving is done using a frontal solver. This is the longest part of process because it requires solving thousands of simultaneous equations.

4. Viscoplastic Models and Results

This chapter provides discussion on the actual finite element models that were studied and the results that were obtained. Section 4.1 contains very simple models containing no cracks, temperature dependence, or thermal strains. These models do not model a semiconductor package, but rather they are provided as checks to show that the viscoplastic subroutines are working correctly. The results are compared to known results that were obtained analytically or by other FEA program. Section 4.2 contains results for the three different flip chip models studied containing viscoplasticity and interfacial cracks.

4.1. Test Models

4.1.1. One element models

In this first example, a model was created consisting of one 20 noded quadratic brick element. This single element was constrained in the x direction on the $x=0$ surface and constrained at one point in y and z directions to prevent solid body movement. Two different types of loading were placed on the element. The first kind was a constant applied load that causes the element to be in constant stress. The second kind of load was an applied constant displacement causing the element to be under constant total strain. The one element model is shown in Figure 4.1. The two loading condition were applied using two different flow rules or constitutive relationships. The first of these is a linear

rule obtained from [20], equation 4.1, where γ is the fluidity parameter and σ is the Von Mises equivalent stress, and σ_y is the yield stress. The second flow rule is the one presented in [2]. This flow rule is used here because it is the same flow rule that will be used in the flip chip models and because it tests the new viscoplastic code's ability to deal with a highly non-linear flow rules and strain hardening. The flow rule is given in equation 4.1 these equations are explained in section 3.3.1.

$$d\varepsilon/dt=\gamma(\sigma-\sigma_y) \tag{4.1}$$

$$\begin{aligned}\frac{d\varepsilon_s}{dt} &= C_1[\sinh(C_2\sigma)]^{C_3}\exp(-C_4/T)\\ \frac{d\varepsilon_c}{dt} &= \frac{d\varepsilon_s}{dt}\left(1+C_5C_6\exp(-C_5\bar{\varepsilon}_{VP})\right)\end{aligned} \tag{4.2}$$

The following four graphs compare results from the new viscoplastic subroutine in FRAC3D with analytical result created using a simple spreadsheet. Figures 4.2 though 4.5 show the results from these tests.

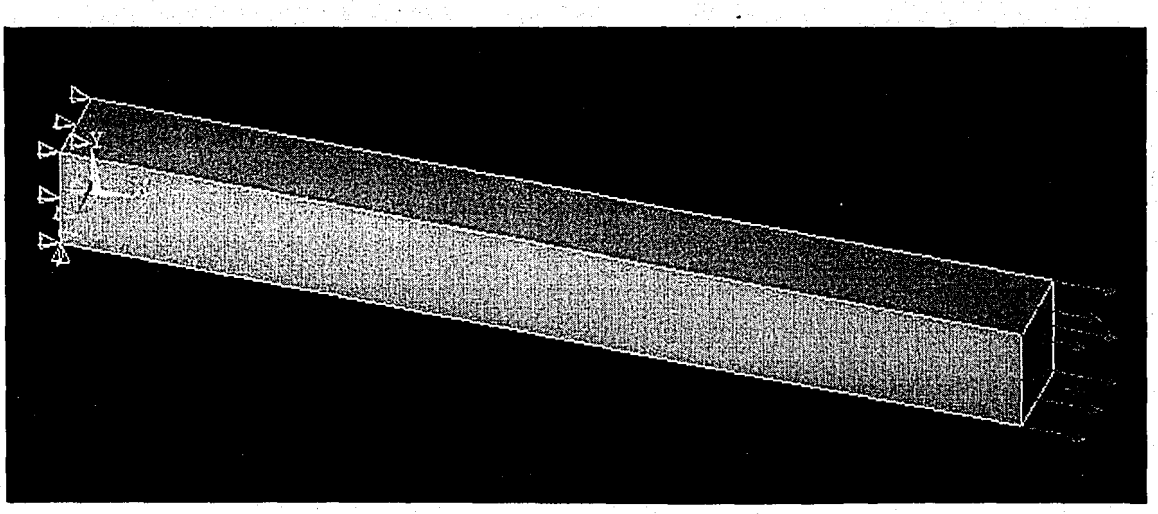

Figure 4.1 One element model

rule obtained from [20], equation 4.1, where γ is the fluidity parameter and σ is the Von Mises equivalent stress, and σ_y is the yield stress. The second flow rule is the one presented in [2]. This flow rule is used here because it is the same flow rule that will be used in the flip chip models and because it tests the new viscoplastic code's ability to deal with a highly non-linear flow rules and strain hardening. The flow rule is given in equation 4.1 these equations are explained in section 3.3.1.

$$d\varepsilon/dt = \gamma(\sigma - \sigma_y) \tag{4.1}$$

$$\begin{aligned} \frac{d\varepsilon_s}{dt} &= C_1[\sinh(C_2\sigma)]^{C_3}\exp(-C_4/T) \\ \frac{d\varepsilon_s}{dt} &= \frac{d\varepsilon_s}{dt}\left(1 + C_5C_6\exp(-C_5\bar{\varepsilon}_{VP})\right) \end{aligned} \tag{4.2}$$

The following four graphs compare results from the new viscoplastic subroutine in FRAC3D with analytical result created using a simple spreadsheet. Figures 4.2 though 4.5 show the results from these tests.

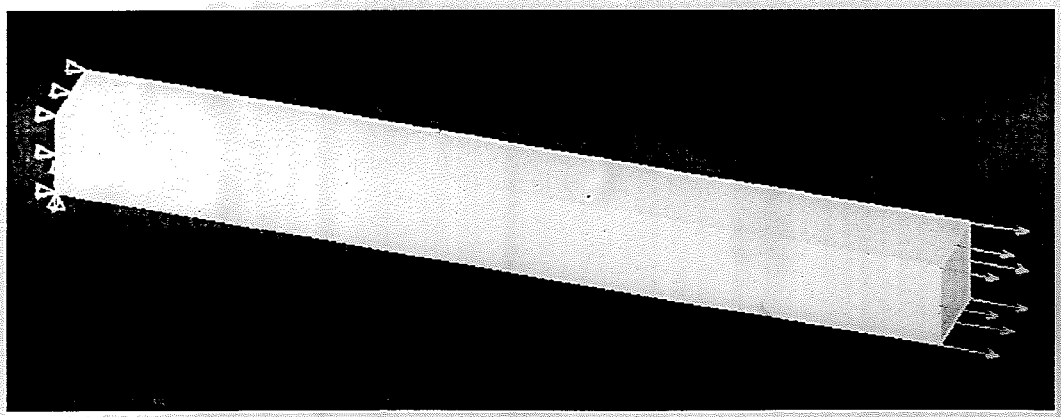

Figure 4.1 One element model

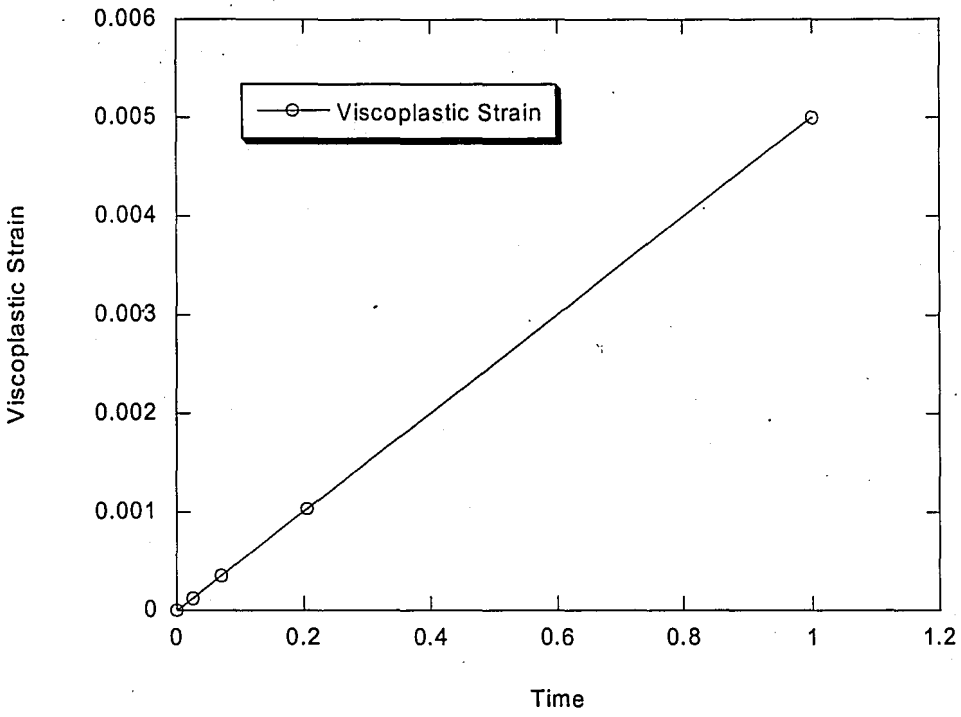

Figure 4.2 Strain caused by constant stress using a linear flow rule

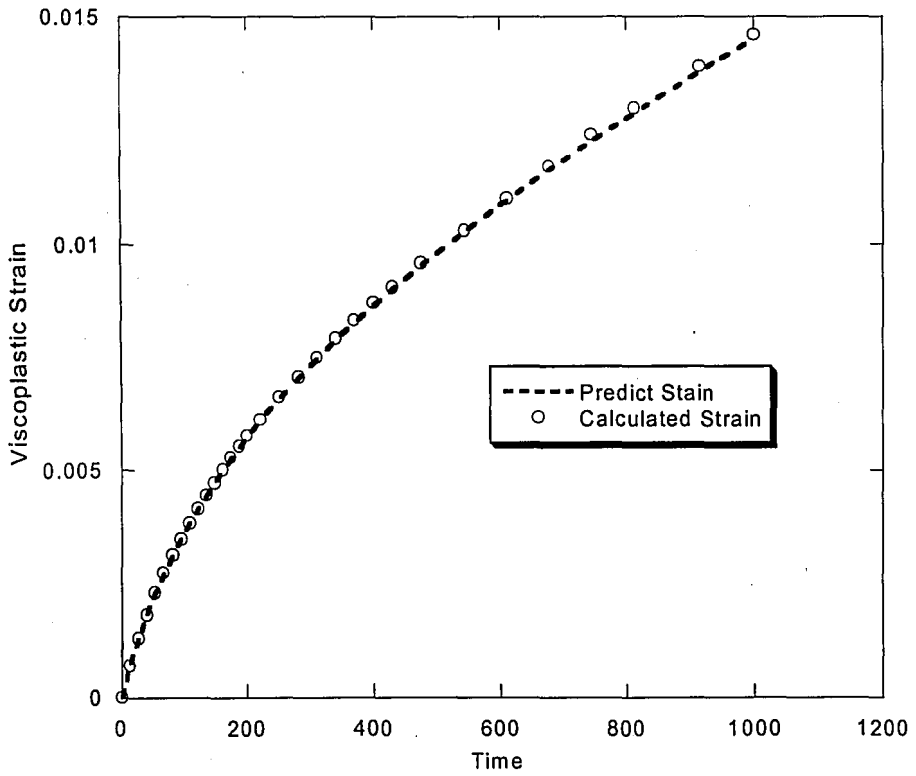

Figure 4.3 Strain caused by constant stress using solder flow rule

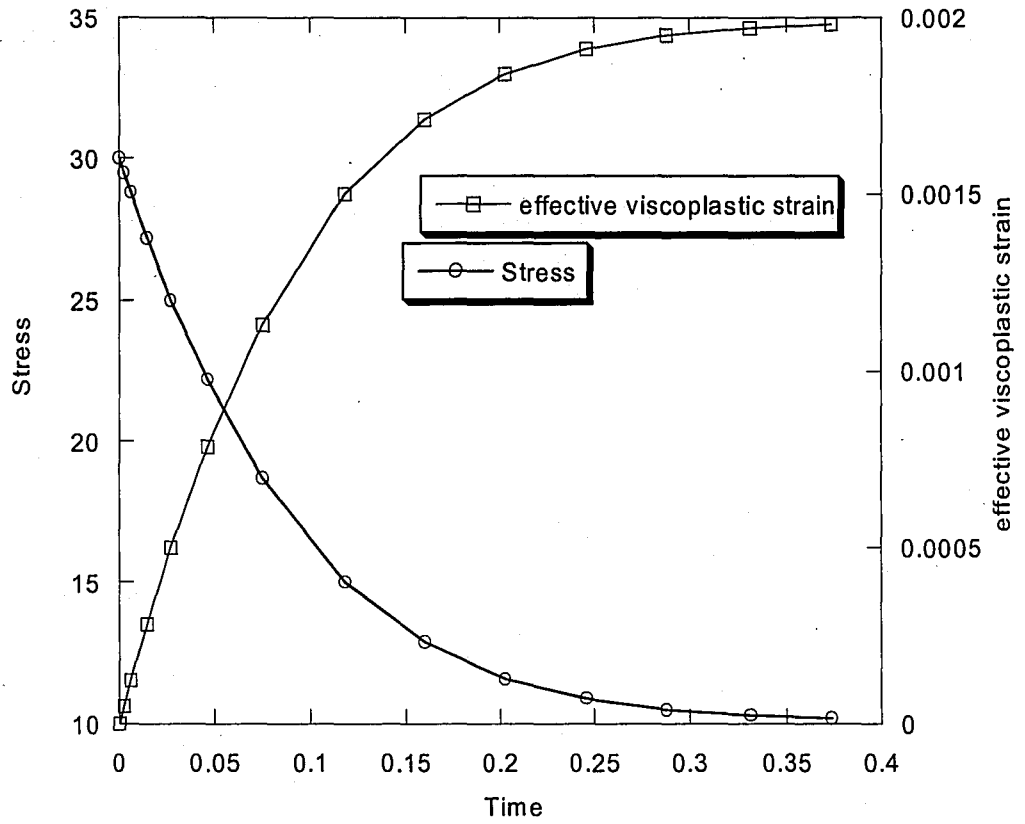

Figure 4.4 Results from Applied Displacement using a Linear Flow Rule

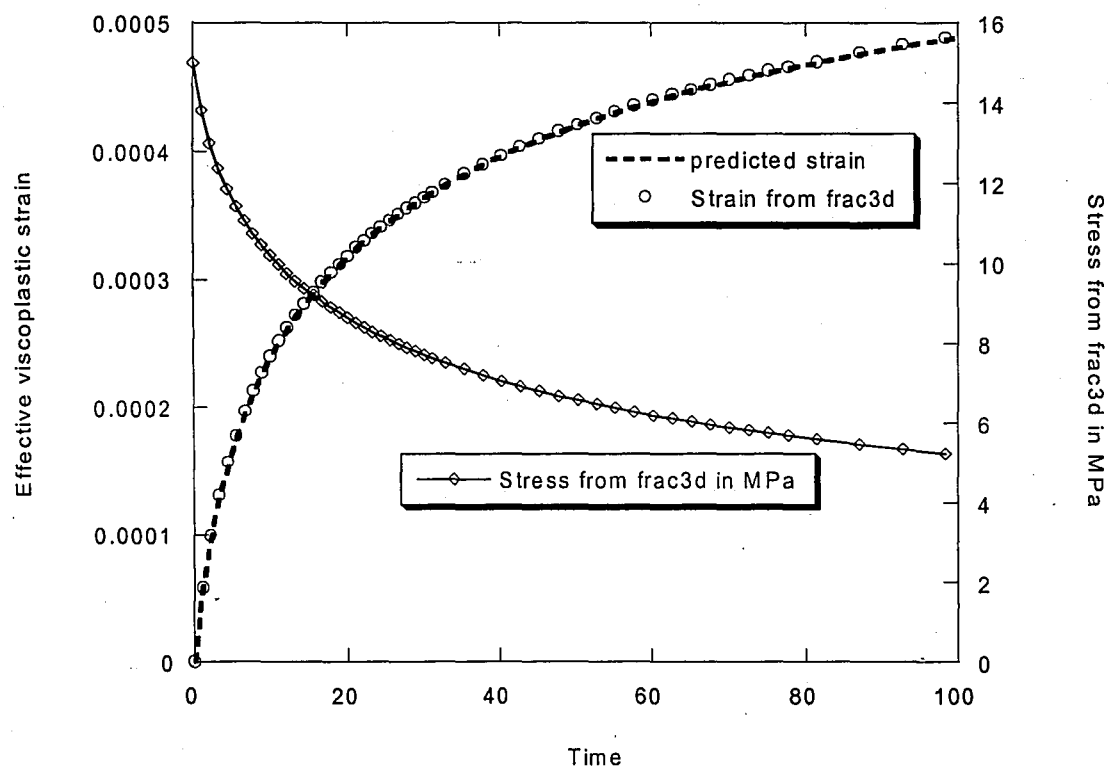

Figure 4.5 Results from Applied Displacement using Solder Flow Rule

4.1.2. Cylinder Model

A quasi-3D model of a pressurized cylinder was used to test the multi-dimensional capability of the code. In this model, a one quarter slice of a cylinder was modeled. The model was constrained completely in the *z*-direction so that it be in plane strain condition. The plane strain condition makes this model essentially the same as a 2D model with same x and y dimensions. This allows the 3D model results to be compared with the results obtain from 2D simulation run using other finite element codes. Figure 4.6 shows a picture of the model created, as is shown, the two ends have symmetry boundary conditions. The model contains 12 elements, which are all 20-noded quadratic bricks.

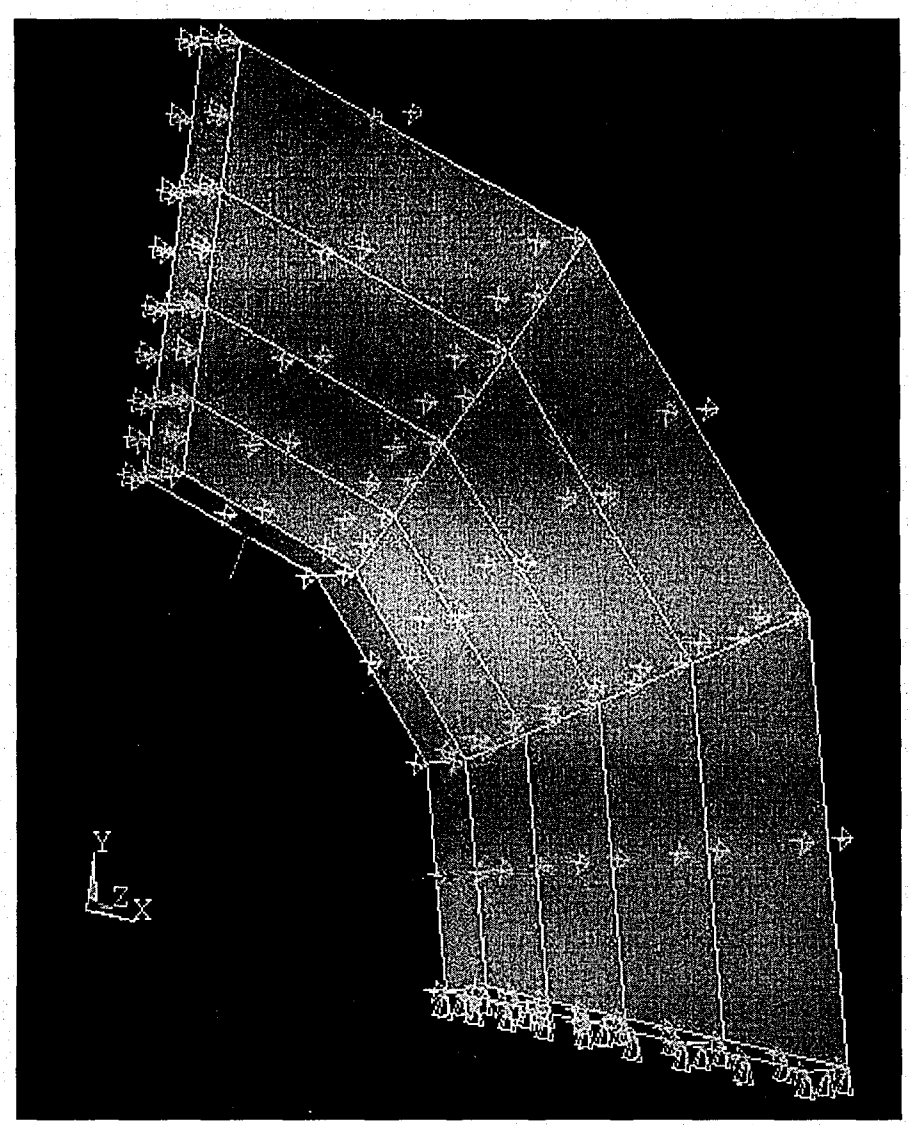

Figure 4.6 Cylinder Mesh with Constraints

The model was run using two different strain laws, the first being a linear strain law identical to the one used in [20]. The equation for the flow rule used is given by equation 4.1 and the problem was rerun with a nonlinear strain law given by equation 4.2. The results obtained using the non-linear flow rule are compared with a 2D ANSYS model. Figure 1.7 provides the results for the linear flow rule from both [20] and from FRAC3D. As the graph shows the results are very similar. Figure 1.8 and 1.9 compare the results of the non-linear flow rule simulation run in ANSYS model and in FRAC3D.

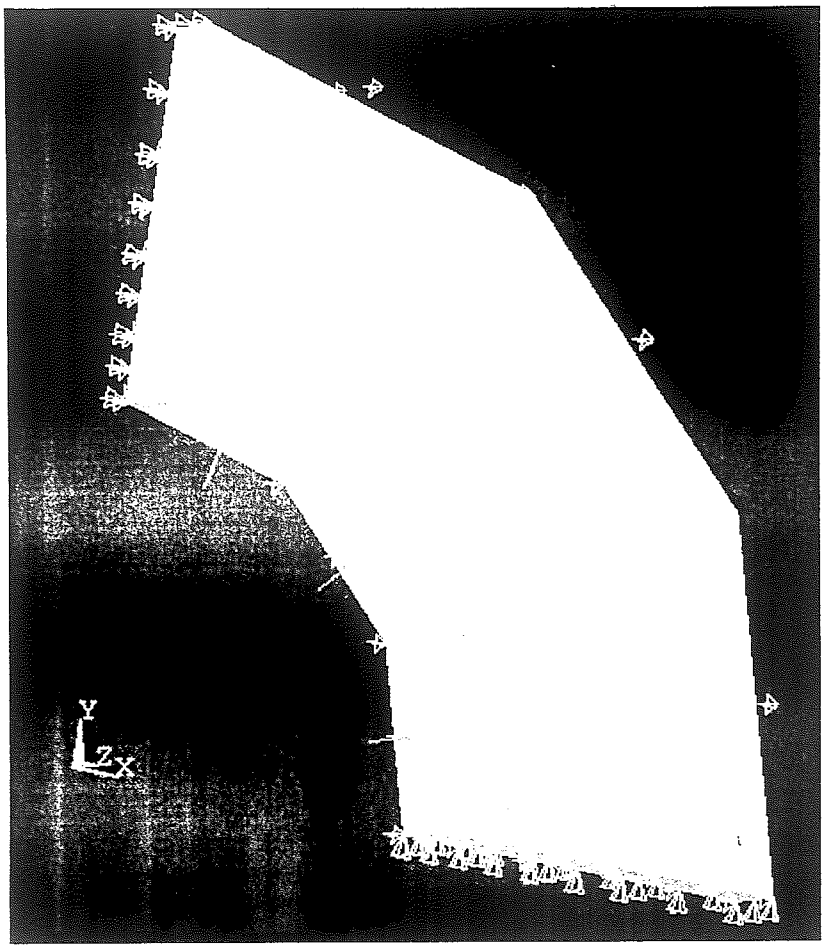

Figure 4.6 Cylinder Mesh with Constraints

The model was run using two different strain laws, the first being a linear strain law identical to the one used in [20]. The equation for the flow rule used is given by equation 4.1 and the problem was rerun with a nonlinear strain law given by equation 4.2. The results obtained using the non-linear flow rule are compared with a 2D ANSYS model. Figure 1.7 provides the results for the linear flow rule from both [20] and from FRAC3D. As the graph shows the results are very similar. Figure 1.8 and 1.9 compare the results of the non-linear flow rule simulation run in ANSYS model and in FRAC3D.

There is some difference, but this is most likely due the different way in which time stepping is controlled in ANSYS model. The discrepancy is not a severe enough difference to suggest an error in the viscoplastic subroutines in FRAC3D.

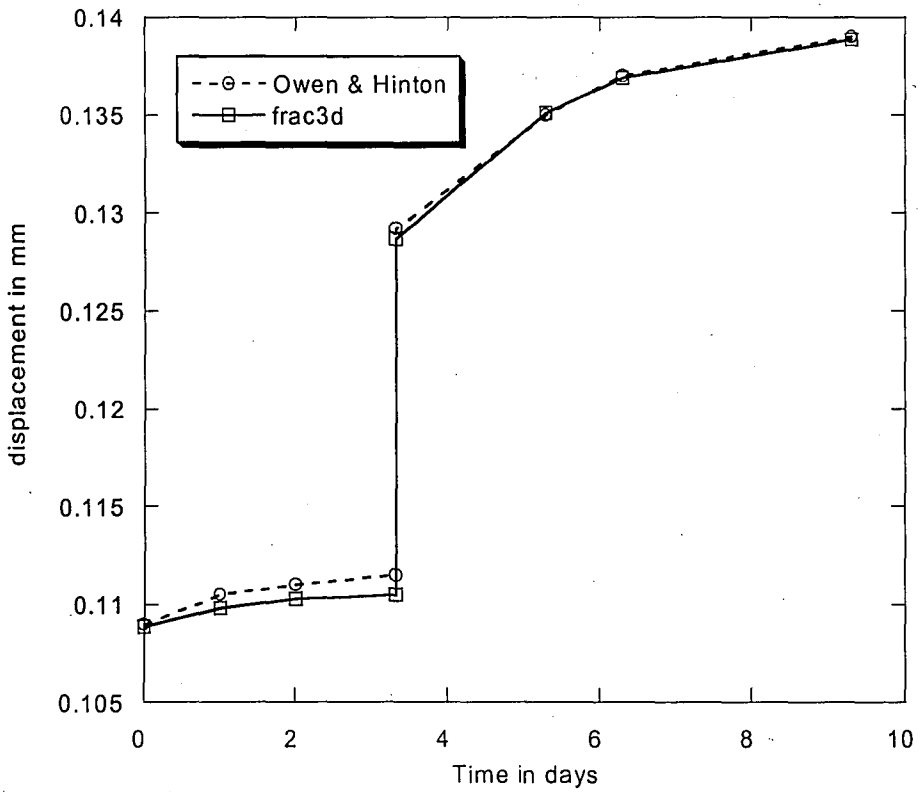

Figure 4.7 Comparison of cylinder results from FRAC3D and Owen & Hinton

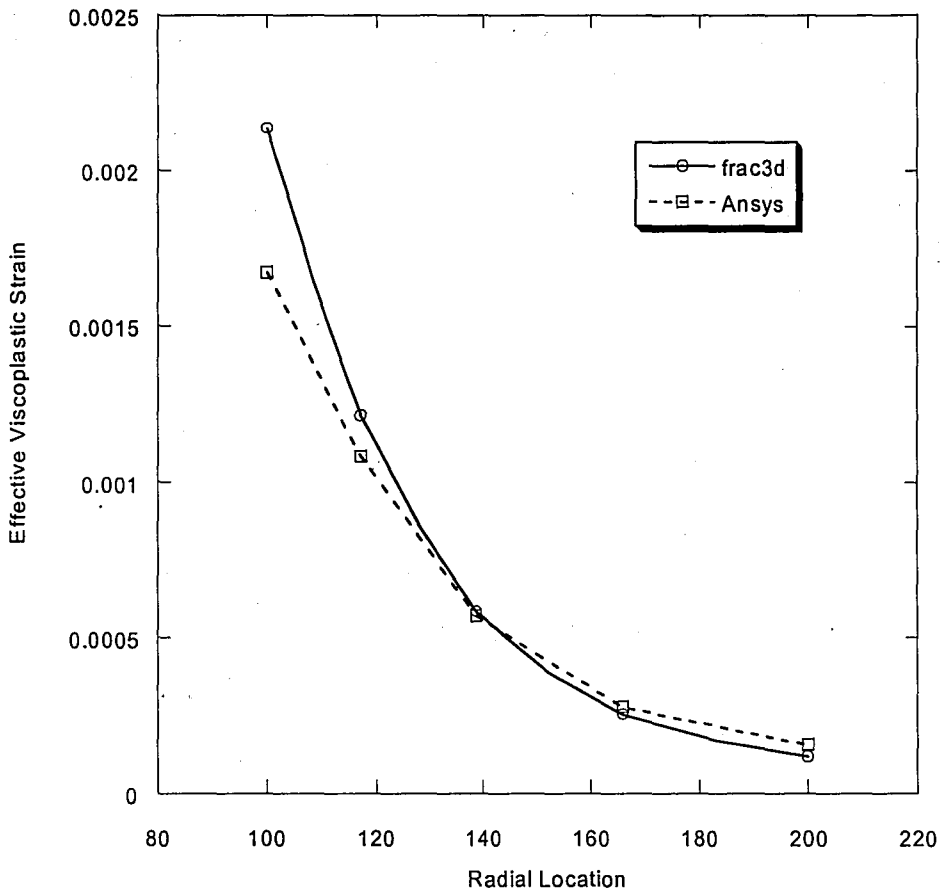

Figure 4.8 Comparison of cylinder results between FRAC3D and ANSYS simulation

4.2. Flip Chip Models

The culmination of this research is the creation of a flip chip model, which contain an interfacial crack and solder modeled viscoplastically. The flip chip model that has been created is a two layered slice model. A two layered slice model was shown to provide reasonably accurate results when compared with a fully 3D model that was shown in chapter 2. The viscoplastic subroutines have been shown to provide reasonably accurate results as shown in section 4.1.

4.2.1. Model Geometry

The model used was a generalized plane strain model with two layers, one of which contains solder bumps and underfill and the other layer contains only underfill between the silicon and substrate layers. The model is intended to model a half diagonal of the chip because the corner is the location where the most severe stress condition exist[3]. The following diagram in Figure 4.9 shows the end of the model where the fillet and solder balls are located. Table 4.1 gives the dimension of all components in the model.

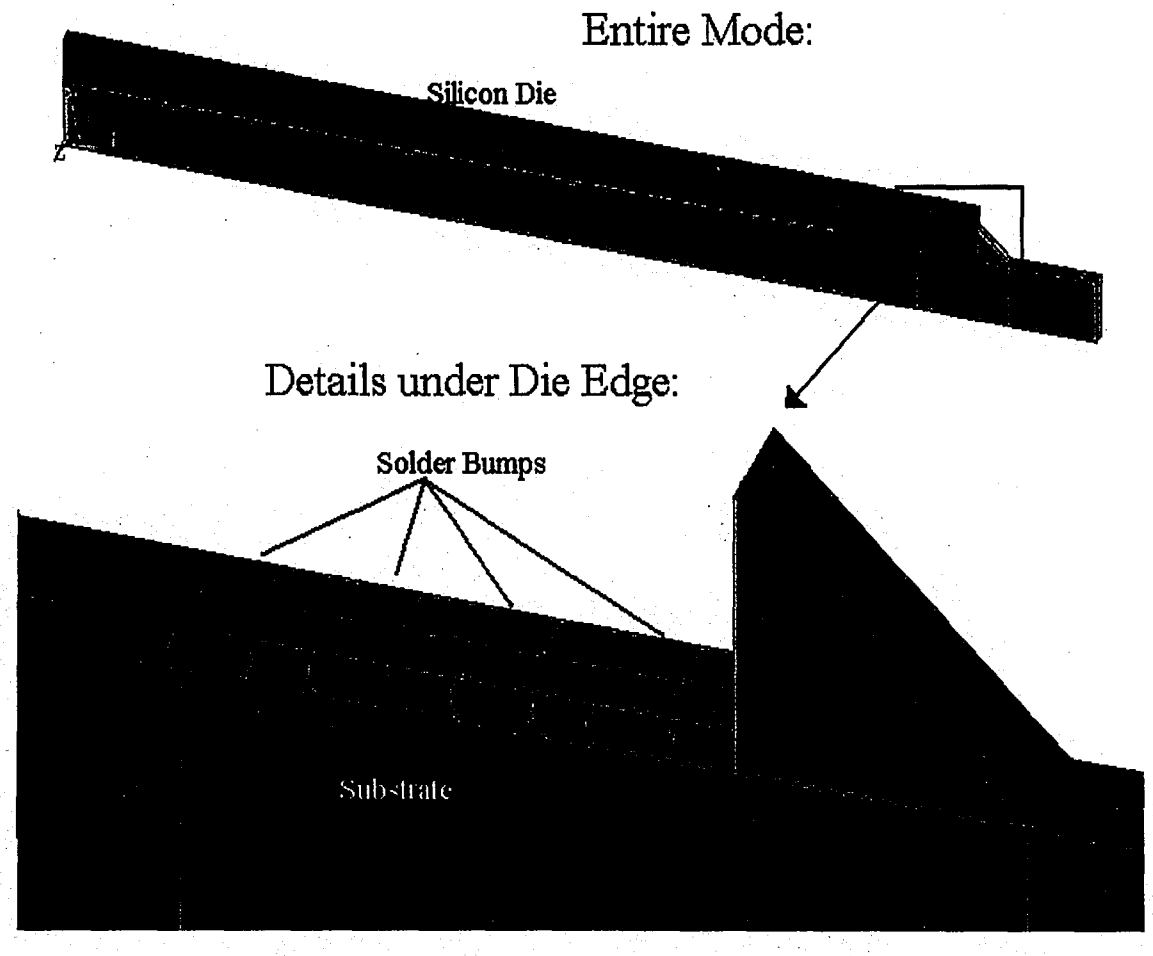

Figure 4.9 Diagram of Two Layer Flip Chip Model with Fillet/Die Crack

Table 4.1 Flip Chip Model Dimensions

Feature	Length in mm	Feature	Length in mm
Die Half Diagonal	14.400	Underfill Layer Thickness	0.100
Substrate Half Diagonal	16.270	Solder Layer Thickness	0.100
Fillet sides	0.381	Solder Bump Diagonal Pitch	0.325
Die Height	0.686	Solder Bump Minimum Width	.100
Substrate Height	1.000	Solder Bump Maximum Width	.140
Underfill/Solder Height	0.076	Crack Length	0.165

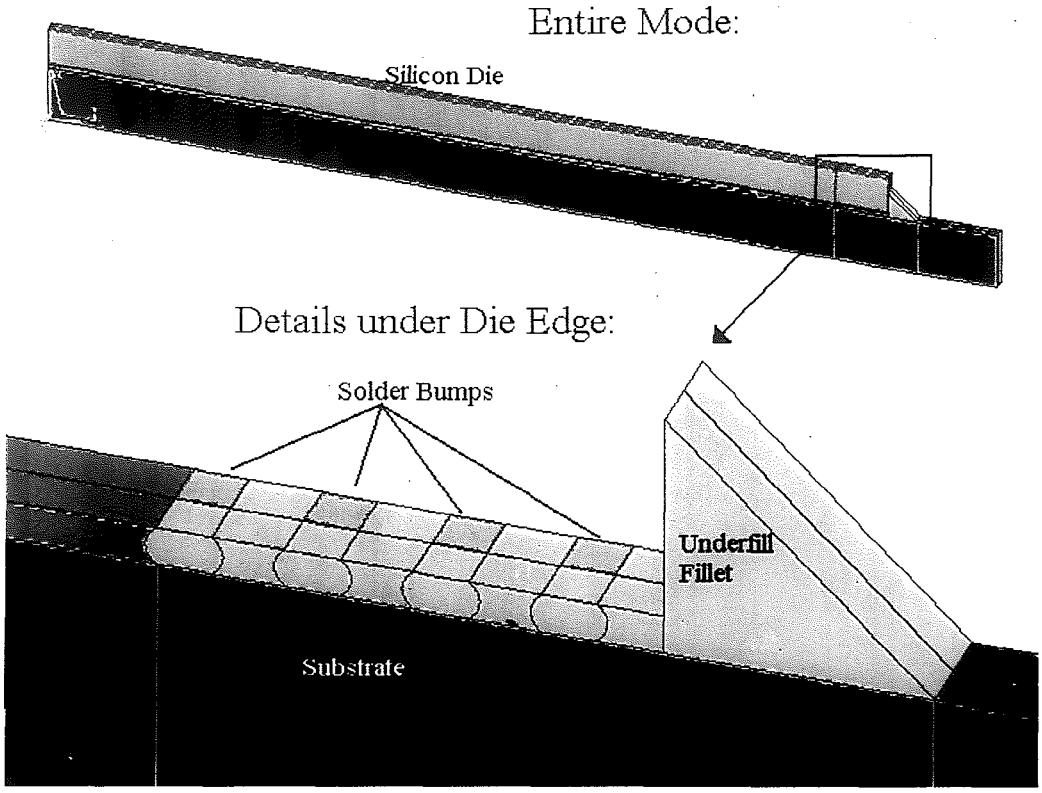

Figure 4.9 Diagram of Two Layer Flip Chip Model with Fillet/Die Crack

Table 4.1 Flip Chip Model Dimensions

Feature	Length in mm	Feature	Length in mm
Die Half Diagonal	14.400	Underfill Layer Thickness	0.100
Substrate Half Diagonal	16.270	Solder Layer Thickness	0.100
Fillet sides	0.381	Solder Bump Diagonal Pitch	0.325
Die Height	0.686	Solder Bump Minimum Width	.100
Substrate Height	1.000	Solder Bump Maximum Width	.140
Underfill/Solder Height	0.076	Crack Length	0.165

4.2.2. Comparison of Viscoplastic, Plastic and Linear Results for Underfill Fillet Crack

The model described in the previous section was run using a thermal loading condition where 150° C is the reference temperature. This reference temperature is chosen because it is close to the cure temperature of underfill and the melting point of solder. A ΔT = - 125° C is applied bringing the temperature down to 25° C at the end of loading. In the plastic and viscoplastic models the solder material behavior is strongly temperature dependent. Since solder acts in a viscoplastic manner the standard .02 % yield stress that would be obtained from a tensile test would depend on strain rate. Given this fact, an estimate for the yield stress was obtained using the viscoplastic strain law. The stress level that would cause a strain of 0.005 in 5 minutes would be considered the yield stress. Table 4.2 lists all linear material properties that were used.

Table 4.2 Flip Chip Elastic Material Properties

	Elastic Modulus in MPa		CTE in 10^{-6} /°C		Poison's Ratio
	At 25 °C	At 150 °C	At 25 °C	At 150 °C	
Silicon	131,000	131,000	2.8	2.8	0.28
Substrate	17,700	14,900	15	15	0.39
Underfill	4,800	2,200	24	49	0.33
Solder	29,600	10,290	23.3	23.3	0.35
Underfill solder mix	11,000	4,200	28	49	0.33

Table 4.3 Solder Yield Strengths for Plastic Analysis

Temp in °C	Yield Strength in MPa
25	26.67
350	11.53
423	4.00

Table 4.4 Solder Viscoplastic flow rule constants (see equation 4.2)

C1	C2	C3	C4	C5	C6
80300	.0670	3.30	8110	263.0	.0230

Figure 4.10 gives the Von Mises stress in the center of the outer most solder ball. Figure 4.10 shows that the viscoplastic and plastic answers are similar. There is some stress relaxation after the loading is complete(the dwell), but this is small in comparison with overall deviation from the linear analysis. In both cases, the increase in stress level is more due to the solder's increased strength as the temperature decreases than it is due to increase in loading or strain hardening. Plastic analysis curve shows the stress level is at the yield stress at every point on the curve. The sharp bend in this curve is due to the way that the yield stress in linearly interpolated by the FRAC3D between the three points at which the yield stress was explicitly defined. Figure 4.11 shows the associated viscoplastic strain for the same node. Notice the plastic and viscoplastic results are also similar in this graph.

The fracture parameters show that the more yielding that occurs in the solder in the model, the lower the strain energy release rate, G, becomes as is shown in figure 4.12. The phase angle values, Ψ, shown in Figure 4.13, shows the mode mixity is not significantly affected by the differences between the plastic and viscoplastic analysis. It is also important to note that the temperature dependence of the underfill properties may be causing some of the variations in Ψ and G.

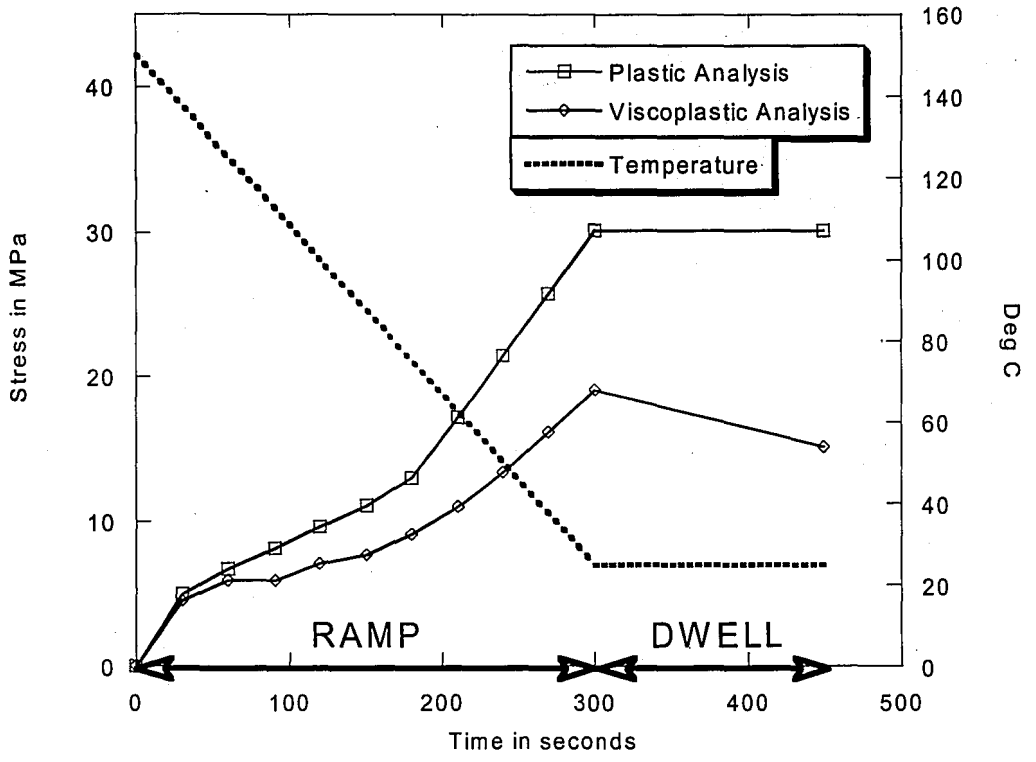

Figure 4.10 Comparison of Von Mises stress between plastic and viscoplastic analysis in the center of outer most solder bump

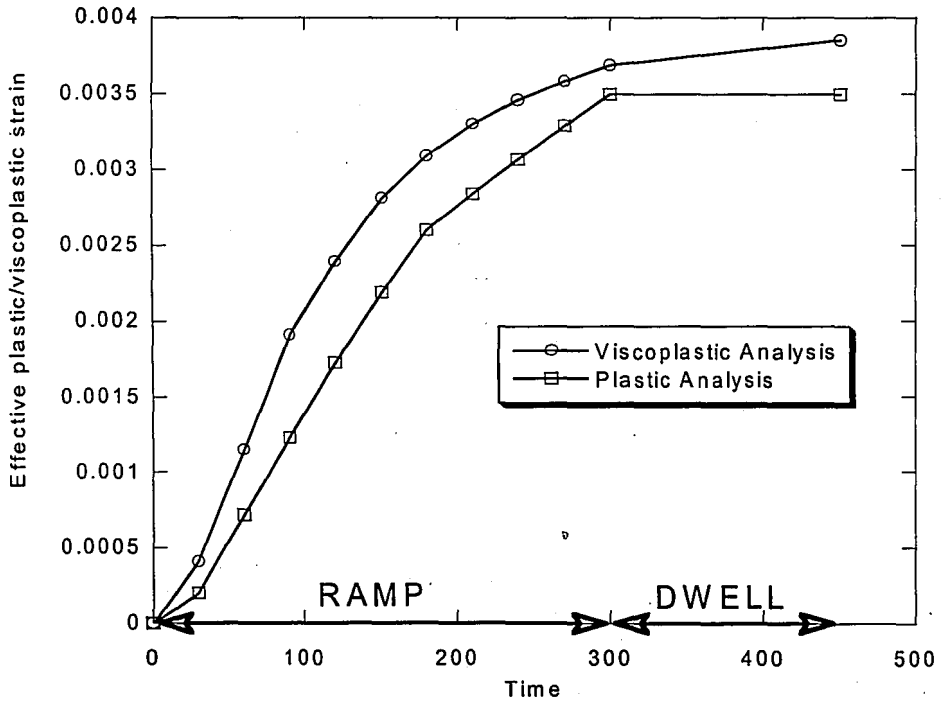

Figure 4.11 Comparision of Plastic Strain between Plastic and Viscoplastic Analysis in the Center of Outer Most Solder Bump

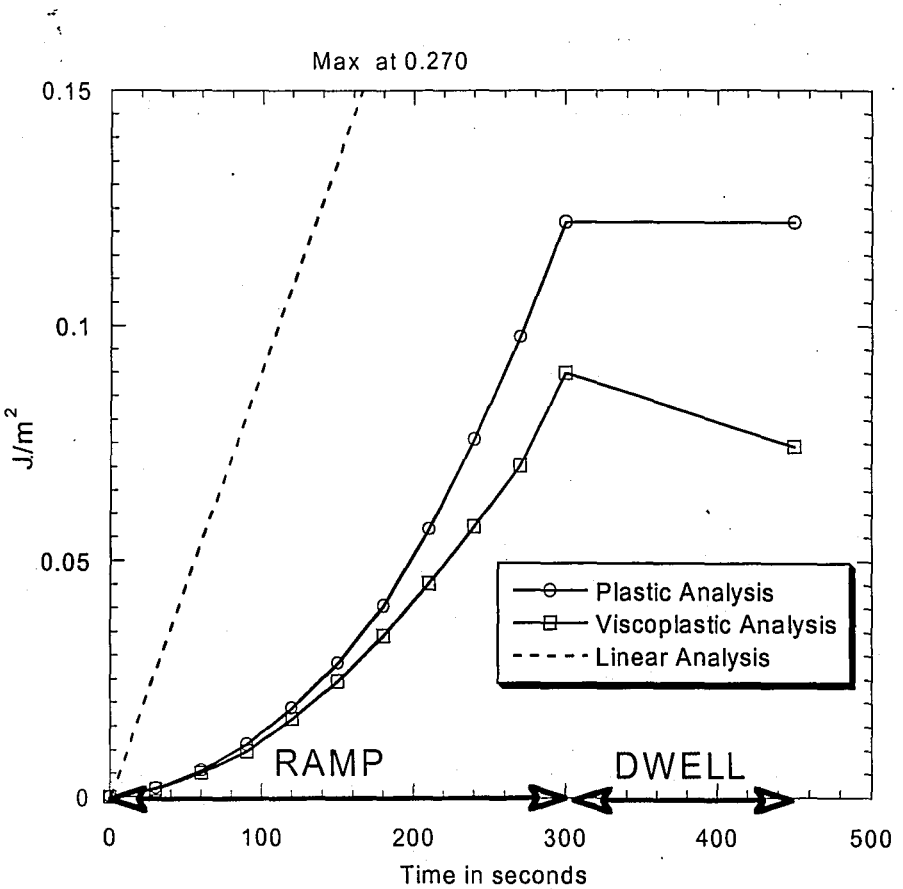

Figure 4.12 Comparison of Strain Energy Release Rate between plastic and viscoplastic analysis

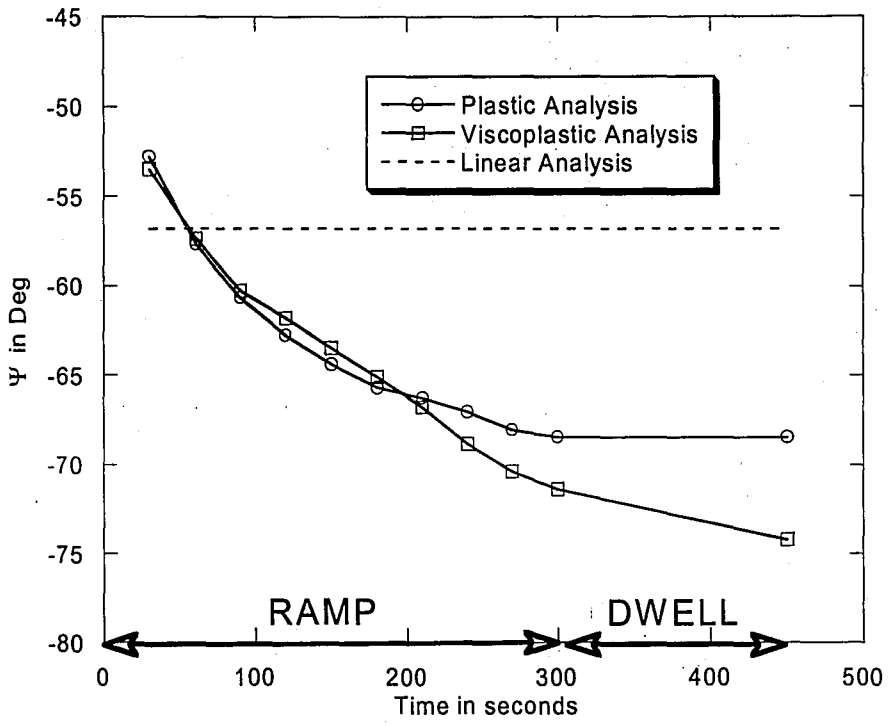

Figure 4.13 Comparison Phase Angle between Plastic and Viscoplastic analysis

4.2.3. Independence of Results from Mesh Density

The viscoplastic deformation and consequent stress in the solder balls is not highly dependent on mesh density. The mesh density was doubled in the model from 2 x 2 to 4 x 4 elements per solder ball. Figure 4.14 and 4.15 show that the stress and viscoplastic strain are nearly identical between the two mesh densities.

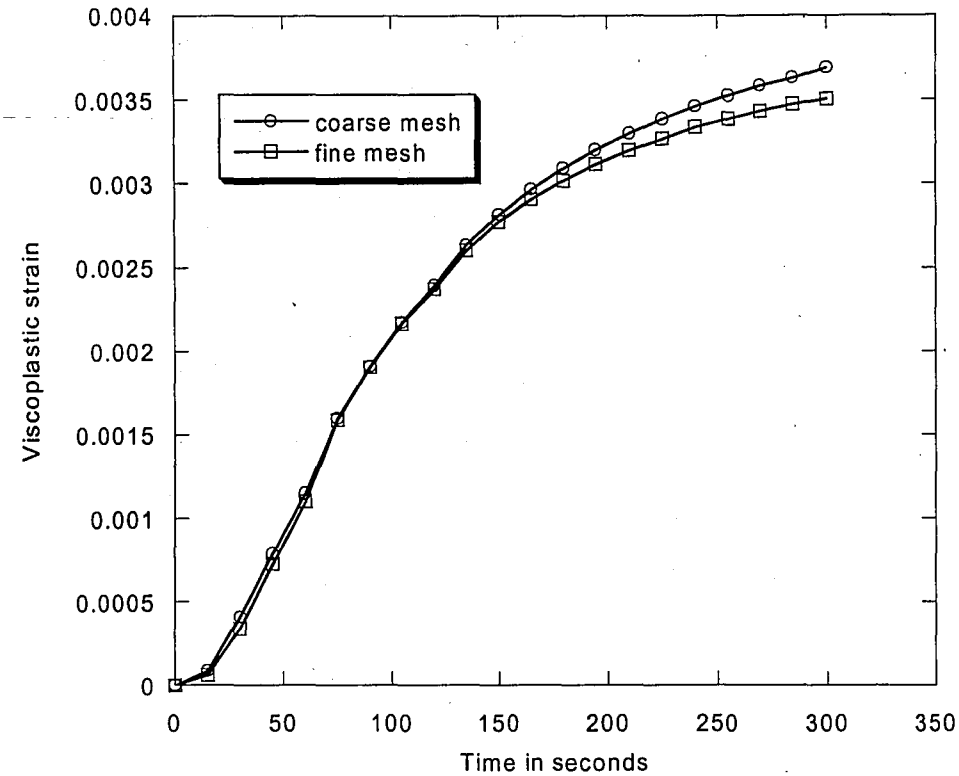

Figure 4.14 Strain Comparison between Coarse and Fine Mesh

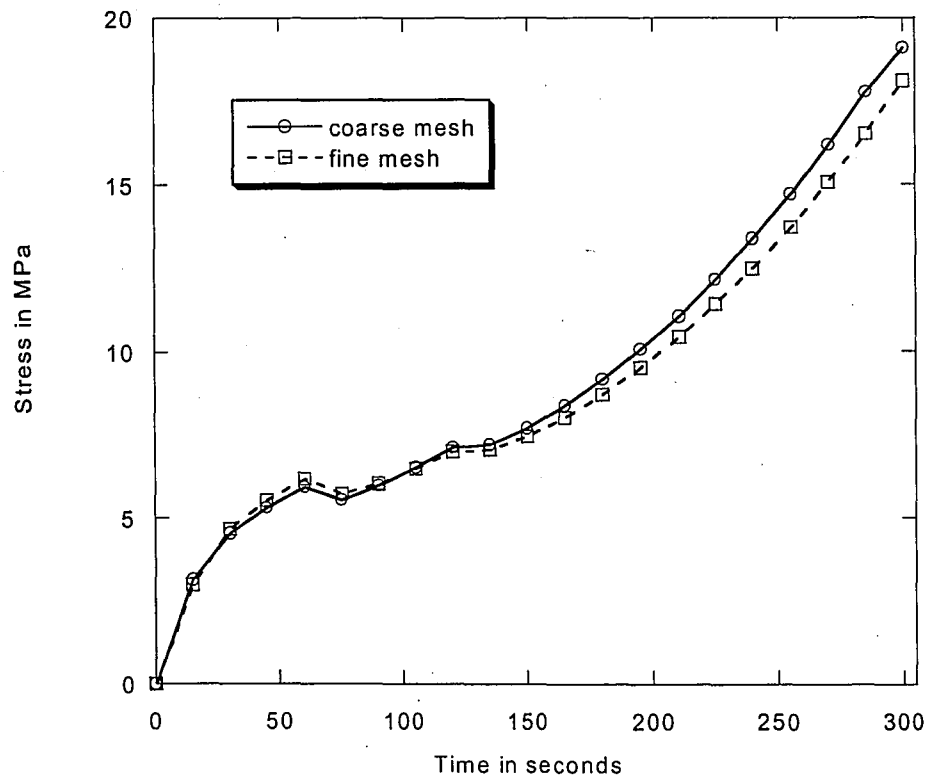

Figure 4.15 Stress Comparison between coarse and fine mesh

4.2.4. Severe Crack Model

A second model was created to simulate a large crack that has propagated past the fillet so that the crack is approaching the outer most solder ball. In this type of crack the interaction between the solder and the crack parameters should be more pronounced. This is definitely the case as is shown in the way the fracture parameters vary over the cross-section. Surprisingly, there is not a significant difference in the viscoplastic strain compared with the less severe crack, when strain is measured at the center of the solder bump. This might have a larger effect if the crack was moved even closer to the outer most solder bump. The results are shown in figure 4.14 and 4.15. The severe crack model does show a much higher strain energy release rate, G, than in the model with a less severe crack. The mode mixity in this model is significantly different from the fillet crack and there is also a much greater variation in G along the crack front than in the first model as is shown in figure 4.18.

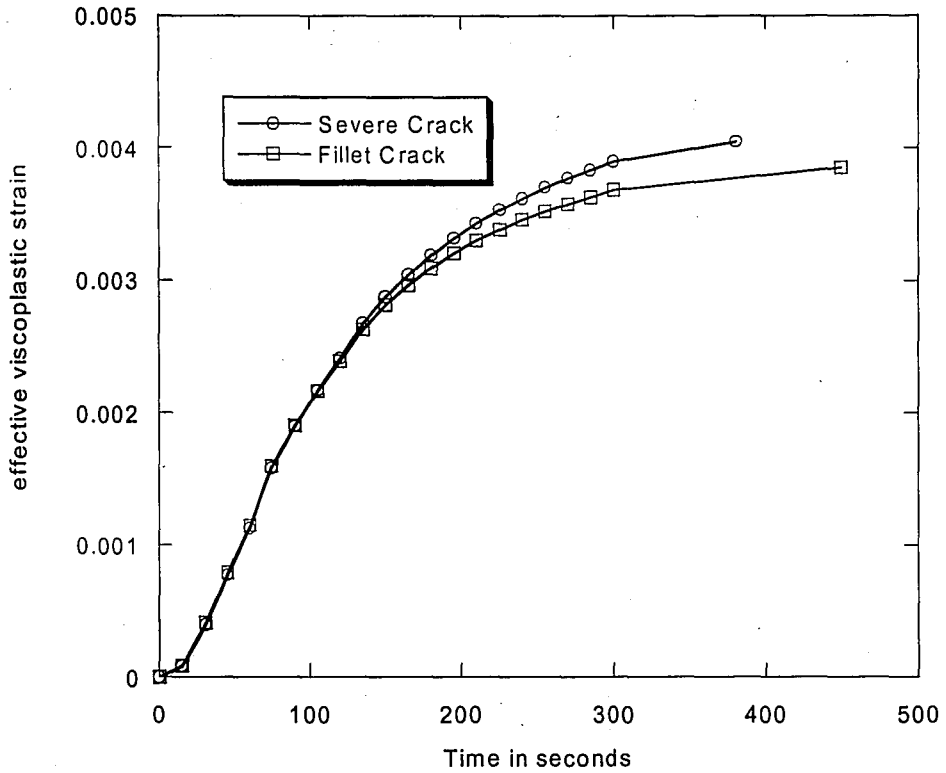

Figure 4.16 Viscoplastic Strain Comparison between Severe and Fillet Crack

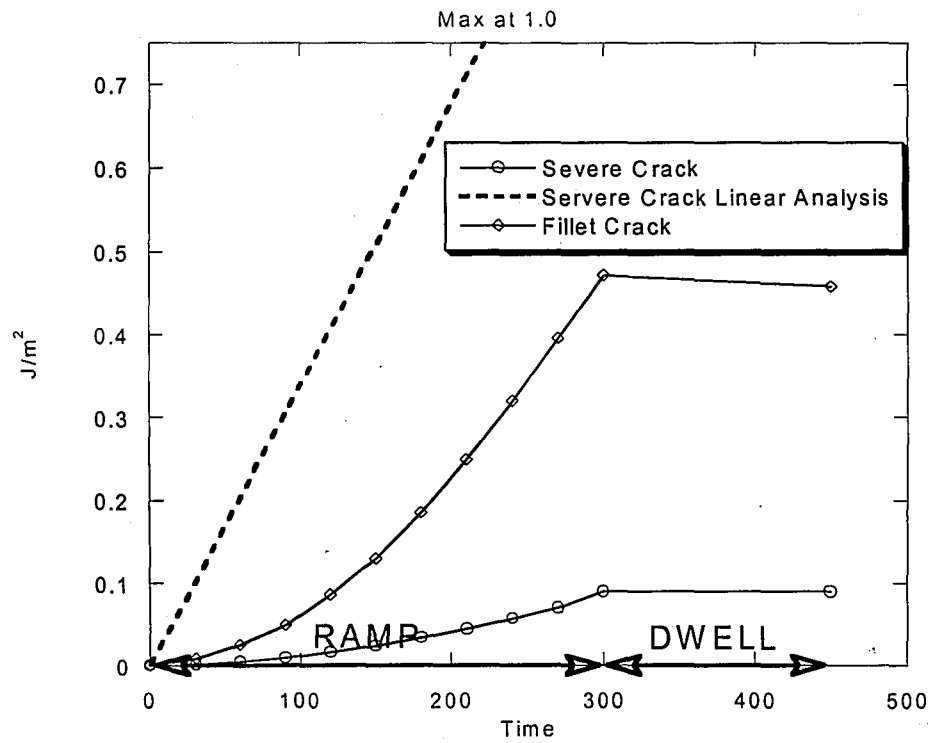

Figure 4.17 Strain Energy Release Rate Comparison between Fillet & Severe Crack

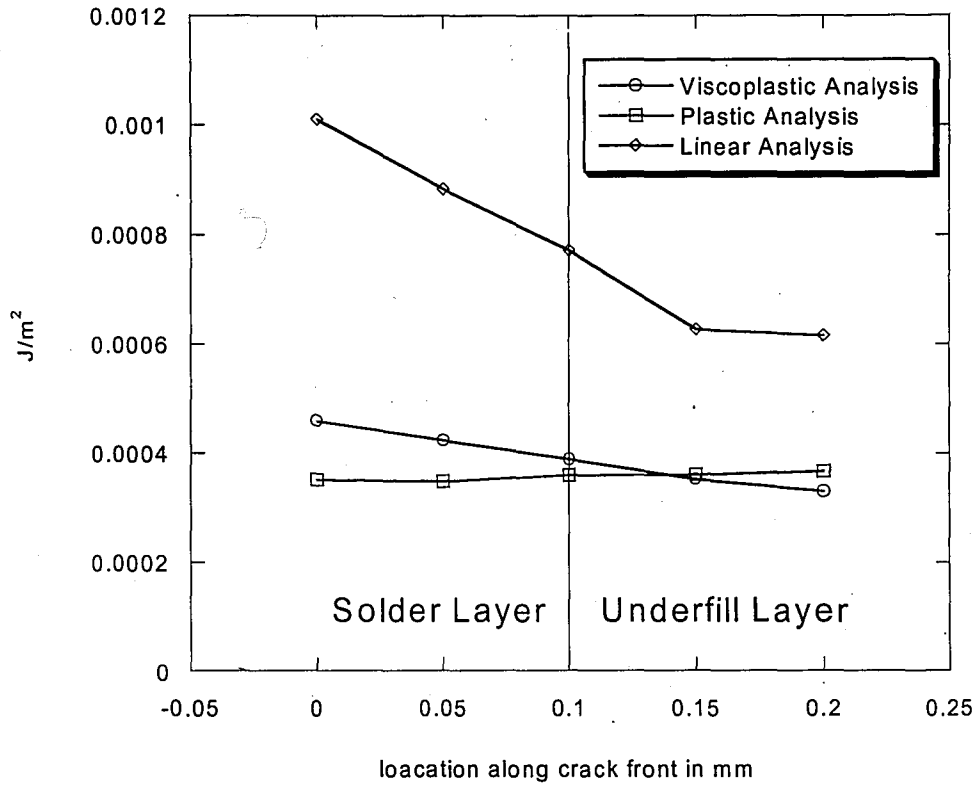

Figure 4.18 Variation in Strain Energy Release Rate along the crack front in Severe Crack model

5. Conclusions

The new viscoplastic capability added to FRAC3D can now be used to more accurately model materials, such as solder, which behave viscoplasticaly. This will lead to more accurate calculation of fracture parameters than with elasto-plastic material properties. The example flip chip models examined in Chapter 4 showed that the differences caused by using non-linear material properties for solder have a great effect on the overall results when compared with linear models results. Implementing the more accurate viscoplasticity materials had a secondary (less pronounced) effect on the overall results. It is believed that this is due to the combination of several. The first factor is that underfill encapsulation compensates for the lost strength of the solder thereby mitigating the effect of the low strength of solder. The second factor is that yield strength values for the plastic simulation were chosen so that they would give the most accurate results for the given problem specification, specifically the total time allowed and the expected severity of the plastic strain. The dwell period did not have a major effect on the strain levels or fracture parameters, because at the end of temperature ramp, the stress levels were not significantly different than the expected long time period values. Even when modeling a severe crack, the results indicated that the underfill continued to hold the layers together, causing similar strain conditions as the less severe cracks.

The accuracy of the two-layer slice model with generalized plane strain provides a reasonably accurate solution when compared with a 1/8 symmetry model. The two layer slice model more accurately matched the 1/8 symmetry model than the 2D plane strain or one-layer generalized plane strain model. Although this was only tested using a BGA

model, and not a Flip Chip model, the geometries share many similarities; therefore, it is believed that the same simplifications are applicable to both models. Two-layer model should continue to be useful in both research and industry. This type of model meets the needs of industry by allowing for quick model generation and solution time. It also meets the researcher's need to more easily study the effect of different types of non-linear or crack growth models that are simulated with many iterations.

5.1. Recommendations for further work

The new viscoplastic capability of the current code would be useful in attempting to model a flip chip that is mounted to a set of viscoplastic solder balls on a printed circuit board (second level attach). This is the most common way in which flip chips are mounted for commercial use. Modeling a flip chip in this way should provide some interesting insight into how the second level attachment affects the fracture parameters and plastic strain results.

6. References

[1] International Microelectronics and Packaging Society, "Flip Chip Workshop" emailed Feb. 2001

[2] Lau, John H., *Ball Grid Array Technology*, McGraw Hill, 1995

[3] Ayhan, Ali "Finite Element Analysis Of Nonlinear Deformation Mechanisms In Semiconductor Packages" Doctoral Dissertation, Lehigh University 2000

[4] Lewis, Dan, conversations June 2000

[5] Darveaux, R., "Solder Joint Fatigue Life Model," in Design & Reliability of Solder and Solder Interconections, Proceedings of the TMS, Orlando, FL, February, 1997

[6] Darveaux, R., "Effect of Simulation Methodology on Solder Joint Crack Growth Correlation," to be presented at the 50th *Electronic Components and Technology Conference 2000*, Las Vegas, NV

[7] Clech, J-P "Solder Reliability Solutions: a PC-Based Design-For-Reliability Tool", *Proceedings, Surface Mount International Conference,* San Jose, Ca, Sept. 10-12, 1996, Vol. I, pp. 136-151

[8] Clech J-P, "Solder Reliability Solutions: form LCCCs to area array assemblies", Proceedings, Nepcon West '96, Anaheim, CA, Feb 1996, pp. 1665-1680.

[9] Anderson, T., Guven I., Madenci E., and Gustasson G., "Necessity of Reexaming Previous Life Prediction Analyses of Solder Joints in Electronic Packages," Proc 2000 *Electronic Components and Technology Conference*

[10] Clech, J-P, "Tools to Assess the Attachment Reliability of Modern Assemblies(BGA, CSP...)", Proc. 1997 Napcon West

[11] Hong, B. Z., and Burrel, L. G., "Nonlinear Finite Element Simulation of Thermoviscoplastic Deformation of C4 Solder Joints in High Density Packaging Under Thermal Cycling," *1994 Inter Society Conference on Thermal Phenomena*, pp. 117-125, 1994.

[12] Gustafsson, G., Guven, I., Kradinov, V. And Madenci, E. 2000, "Finite Element Modeling of BGA Packages for Life prediction," to be presented at the 50th *Electronic Components and Technology Conference*, Las Vegas, NV

[13] Chandran, B., Goyal, D., Thomas, J., "Effect of Package Design and Layout on BGA Solder Joint Reliability of an Organic C4 Package," Proc. 2000 ECTE

[14] Pang, John H. L., Tan, Tze-Ing, and Sitaraman, Suresh K., "Thermo-Mechanical Analysis of Solder Joint Fatigue and Creep in a Flip Chip On Board Package Subjected to Temperature Cycling Loading," *1998 Electronic Components and Technology Conference*, IEEE, pp. 878-883.

[15] Clech, J-P, "Flip Chip/CSP Assembly Reliability and Solder Volume Effects" Proc 1998 Surface Mount International Conference, San Jose, CA

[16] Goodelle, Jason, conversations July 2000

[17] Kalinis, Arturus, Finite Element Analysis, Class Notes, Fall 2000

[18] Cook, R. D., Malkus, D. S. and Plesha, M. E., "Concepts and Applications of Finite Element Analysis", John Wiley & Sons, 1989.

[19] Boresi, Arthur *Advanced Mechanics of Materials* Fifth Edition, Chapter 17, John Wiley & Sons Inc, 1993

[20] Owen, D. R. J., and Hinton, E., *Finite Elements in Plasticity*, Pineridge Press, 1980.

7. Appendices

7.1. Glossary of Abbreviations

BGA	Ball Grid Array
BT	Bismaleimide triazine (composite material)
CSMR	Comprehensive Surface Mount Reliability
CSP	Chip Scale Package
CTE	Coefficient of Thermal Expansion
d.o.f.	Degrees of freedom
FCOB	Flip Chip on Board
FE	Finite Elements
FEA	Finite Elements Analysis
FFT	Failure Free Time
FR-4	A type of glass-filled epoxy composite
IC	Integrated Circuit
LCCC	Leadless Ceramic Chip Carriers
NSMD	Non-SMD
PBGA	Plastic Ball Grid Array
PCB	Printed Circuit Board
PWB	Printed Wire Board
SMD	Solder Mask Defined
SMT	Surface mount technology
SRS	Solder reliability Solutions
Tg	Glass Transition Temperature
TSOP	Thin Small Outline Package
QFP	Quad Flat Package
C4	Controlled Collapse Chip Connection
ECTC	Electronic Components and Technology Conference

8. Vita

Marc Heffes was born August 16, 1978 in New York, New York to Albert and Sharon Heffes. Soon after, the family moved to New City, NY where he grew up and attended High School at Clarkstown North until 1996. In 1996, Marc was admitted to Lehigh University where he studied engineering and had internships with Rexroth Corp, Ingersoll-Rand and Lucent Technologies. In June 2000, Marc graduated with High Honors receiving a B.S. in Mechanical Engineering, which also earned him a scholarship to continue studying at Lehigh. Wasting no time, he continued his studies in Mechanical Engineering hoping to earn his Master's of Science degree in only one year.

END OF TITLE